Translation profiling of stress-induced small proteins reveals a novel link among signaling systems

Sangeevan Vellappan[1,2,3], Junhong Sun[1], John Favate [2,3], Pranavi Jagadeesan[1], Debbie Cerda[1,2], Premal Shah [2,3], Srujana S. Yadavalli[1,2]*
[1]Waksman Institute of Microbiology, Rutgers University, Piscataway, NJ USA
[2]Department of Genetics, School of Arts and Sciences, Rutgers University, Piscataway, NJ USA
[3]Human Genetics Institute of New Jersey, Rutgers University, Piscataway, New Jersey, USA

*Corresponding author
Waksman Institute of Microbiology
Rutgers University
190 Frelinghuysen Rd
Piscataway NJ 08854
Phone: 848-445-0251
Email: sam.yadavalli@rutgers.edu

Abstract

Signaling networks allow adaptation to stressful environments by activating genes that counteract stressors. Small proteins (≤ 50 amino acids long) are a rising class of stress response regulators. *Escherichia coli* encodes over 150 small proteins, most of which lack phenotypes and their biological roles remain elusive. Using magnesium limitation as a stressor, we identify stress-induced small proteins using ribosome profiling, RNA sequencing, and transcriptional reporter assays. We uncover 17 small proteins with increased translation initiation, several of them transcriptionally upregulated by the PhoQ-PhoP two-component signaling system, crucial for magnesium homeostasis. Next, we describe small protein-specific deletion and overexpression phenotypes, underscoring their physiological significance in low magnesium stress. Most remarkably, we elucidate an unusual connection via a small membrane protein YoaI, between major signaling networks – PhoR-PhoB and EnvZ-OmpR in *E. coli*, advancing our understanding of small protein regulators in cellular signaling.

Keywords

Stress response / translation-profiling / small proteins / magnesium starvation / bacterial signaling

Synopsis

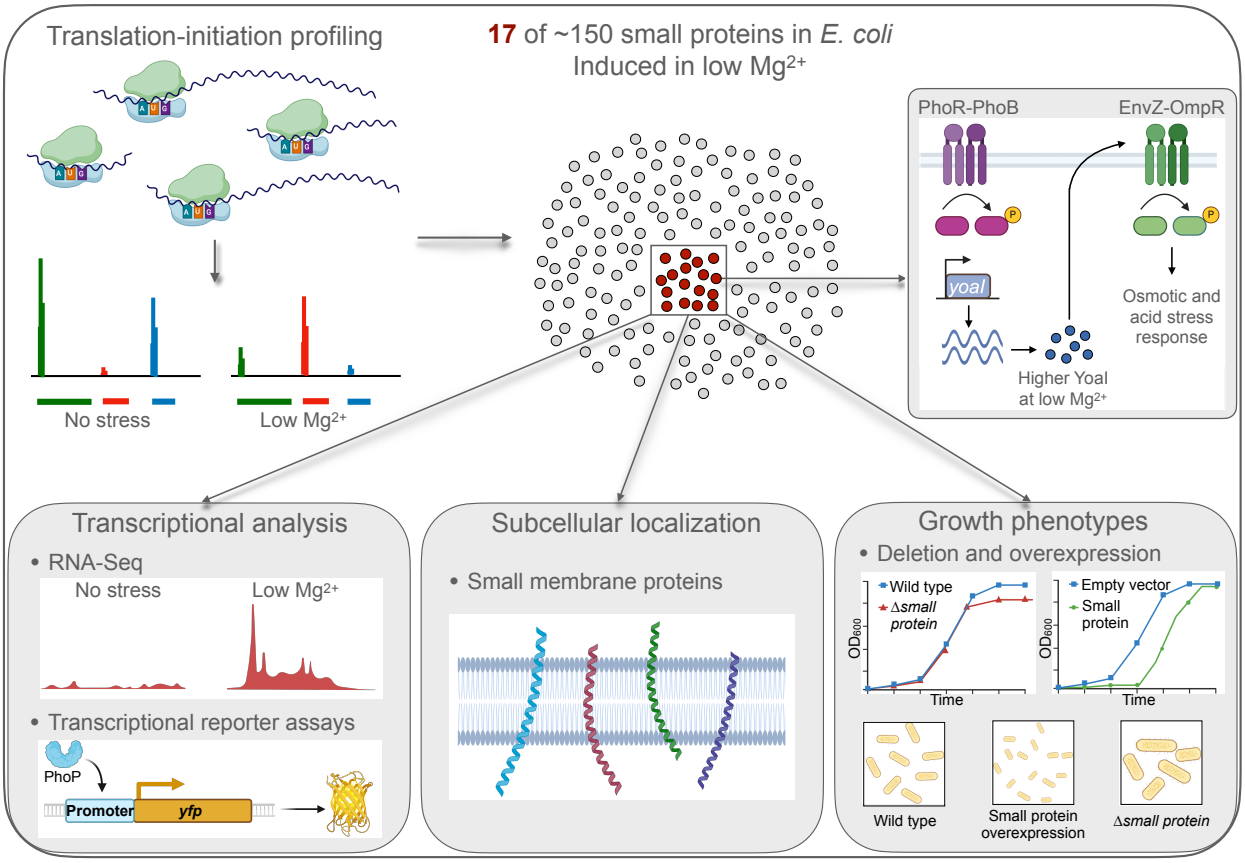

- Ribo-RET identifies 17 small proteins induced under low magnesium (Mg^{2+}) stress in *E. coli*
- Many of these proteins are transcriptionally activated by PhoQP signaling system
- Half of the stress-induced small proteins localize to the membrane
- Deletion or overexpression of specific small proteins affects growth under stress
- Small protein YoaI connects PhoR-PhoB and EnvZ-OmpR signaling networks

Introduction

Living organisms sense and respond to environmental stressors through a wide variety of gene regulatory mechanisms (Carlberg & Molnar, 2016). In bacteria, signal transduction is primarily carried out by two-component signaling systems (Goulian, 2010; Stock *et al*, 2000; Laub, 2014). Gene expression regulation can occur at various stages including transcription, post-transcription, translation, and post-translation (Baumberg, 1999; Banerjee, 2022; Tollerson & Ibba, 2020; Cain *et al*, 2014). While some of these mechanisms involving regulators such as transcription factors and small RNAs have been extensively studied (Gottesman, 2019; Storz *et al*, 2011; Seshasayee *et al*, 2011), other regulatory pathways essential for stress adaptation remain less well understood. Small proteins (≤50 amino acids in prokaryotes and ≤100 amino acids in eukaryotes), encoded by authentic small open reading frames, are emerging as key

regulators of stress response (Burton *et al*, 2024; Hemm Matthew R. *et al*, 2020; Yadavalli & Yuan, 2022), highlighting a need for further investigation into their roles and mechanisms of action.

Advances in bioinformatics, gene expression studies, and ribosome profiling have identified hundreds of previously unannotated small proteins in all kingdoms of life including humans (Hemm Matthew R. *et al*, 2020; Gray *et al*, 2022; Pueyo *et al*, 2016; Patraquim *et al*, 2020; Sberro *et al*, 2019; Kastenmayer *et al*, 2006; Steinberg & Koch, 2021). In *Escherichia coli,* more than 150 small proteins have been documented (Hemm Matthew R. *et al*, 2020; Gray *et al*, 2022). While there has been significant progress in identifying small proteins, a major gap in our knowledge is the lack of understanding of the functions of most of these proteins (Gray *et al*, 2022; Burton *et al*, 2024). Small proteins are typically non-essential, at least under standard growth conditions used in the labs, and their requirement is likely conditional when the activity of a larger target needs fine-tuning. In support of this idea, it was previously observed that some small proteins accumulate at higher levels in a specific growth phase, medium, or stress condition (Hemm *et al*, 2008, 2010). Magnesium (Mg^{2+}) is an important cofactor affecting the catalysis and stability of numerous proteins and RNAs involved in vital cellular processes, including translation (Groisman & Chan, 2021). Given the central role of Mg^{2+}, its deprivation poses a major stress to the cells. The signal transduction and physiological response to low Mg^{2+} is fairly well understood, which involves the activation of the master regulator, PhoQP two-component signaling system in gammaproteobacteria (Groisman *et al*, 2021; Groisman & Chan, 2021; Groisman, 2001).

So far, three small proteins are known to mediate stress response to magnesium limitation in bacteria. Firstly, MgrB, a 48-aa transmembrane protein negatively regulates the sensor kinase PhoQ of the PhoQP signaling system (Yadavalli Srujana S. *et al*, 2020; Lippa & Goulian, 2009). During magnesium starvation, the absence of MgrB leads to hyperactivation of the PhoQP pathway, resulting in cell division inhibition and filamentation in *E. coli* (Yadavalli *et al*, 2016). In addition to its role in Mg^{2+} stress, loss of MgrB in *E. coli* increases tolerance to trimethoprim, an antibiotic commonly used to treat bacterial infections (Patel & Matange, 2021). In clinical isolates of *Klebsiella pneumoniae*, disruption of MgrB-mediated inhibition of PhoQ also leads to acquired colistin resistance (Cannatelli *et al*, 2014). A second small membrane protein, MgtS is also induced under low Mg^{2+} stress and is important for magnesium homeostasis (Wang *et al*, 2017; Yin *et al*, 2019). MgtS protects the magnesium transporter, MgtA, from degradation when Mg^{2+} is limited (Wang *et al*, 2017). PmrR is the third small membrane protein shown to be expressed under low Mg^{2+} stress in *Salmonella enterica* (Kato *et al*, 2012; Hong *et al*, 2018). PmrR is activated by the PmrAB two-component system (Chen *et al*, 2021; Kato *et al*, 2012; Tian *et al*, 2021) in a PhoP-dependent manner and inhibits the lipopolysaccharide modification enzyme, LpxT.

Here we ask, what subset of the ~150 small proteins in *E. coli* are induced under magnesium limitation? We hypothesized that, like MgrB, MgtS, and PmrR, many other small proteins with potential regulatory roles are yet to be identified as part of this stress response. We leveraged the translation-initiation profiling method, Ribo-RET (Meydan *et al*, 2019; Weaver *et al*, 2019) to

identify small proteins induced by low magnesium stress, revealing a set of 17 proteins representing a substantial proportion (~11%) of the documented small proteins in *E. coli*. To investigate the transcriptional regulation of the stress-induced small proteins, we utilized RNA-Seq and transcriptional reporter assays, we investigated the transcriptional regulation of these stress-induced small proteins, shedding light on the genomic regions responsible for their expression and discerning any regulatory influence from the PhoQP system. Additionally, using epitope-tagging, microscopy, and biochemical analysis, we meticulously examined the localization, overexpression, and loss-of-function phenotypes of these small proteins. Through these experiments, we unexpectedly uncovered how the small membrane protein YoaI, transcriptionally controlled by the PhoRB signaling pathway (Gardner & McCleary, 2019), displays increased protein levels under magnesium stress and activates another well-studied two-component system EnvZ-OmpR (Kenney & Anand, 2020) in *E. coli*.

Results

Identification of low magnesium stress-induced small proteins in *E. coli* using translation-initiation profiling

To identify small proteins that accumulate under low magnesium stress, we adapted the translation initiation profiling method called Ribo-RET (Fig. 1A) – a modified ribosome profiling approach utilizing translation initiation inhibitors for the identification of small proteins in bacteria (Cope *et al*, 2022). Retapamulin (RET) is an antimicrobial compound that can stall ribosomes at the translation start sites to help identify previously unannotated open reading frames (Meydan *et al*, 2019; Weaver *et al*, 2019). In this study, we prepared Ribo-RET libraries of wild-type *E. coli* cells grown in media with or without magnesium to examine small proteins expressed in response to magnesium starvation.

In our Ribo-RET data, we observe an increase in reads mapping to a specific distance of the ribosomal P-site codon from the 3' end of the reads in our libraries, ~6-10 nucleotides (nt) downstream of the expected start codon (Fig. S1), similar to the pattern observed in previous translation initiation profiling studies (Weaver *et al*, 2019). We calculated ribosome density at annotated translation initiation sites using reads mapped from 4 to 20 nt downstream of the first nucleotide in the start codon, using a broad window of 16 nt to capture all relevant footprint sizes. In our analysis, the ribosome footprint sizes range from 16-24 nt, as illustrated in Fig. S1, as anticipated for the bacterial systems (Glaub *et al*, 2020).

The PhoQP signaling system is upregulated under Mg^{2+} limitation (Kato *et al*, 1999) (Fig. S2A-B). As expected, the read counts at the translation start site for PhoP and PhoQ were more than 4-fold and 10-fold higher, respectively, under stress conditions compared to no stress. Three small proteins known to be induced under low Mg^{2+} stress – MgrB, MgtS, and PmrR, show a 9-fold, 5-fold, and 5-fold increase in the reads mapping to the translation start sites, respectively, under stress vs. no stress (Fig. 1B-C, S2C). Overall, in our Ribo-RET data, we see a moderate correlation between the reads mapping to the start sites of all proteins expressed under these two conditions (Fig. 1C), which is indicative of the anticipated changes in the translation initiation of proteins during stress response.

We detected 379 proteins with ≥3-fold increase in read counts under stress, several among these are small proteins <50 aa in length (Table S4). We narrowed down a set of 17 small proteins namely MgtS, MgrB, PmrR, MgtT, YmiC, YmiA, YoaI, YobF, YddY, YriB, YadX, YkgS, YriA, YdgU, YqhI, YadW and DinQ for further analysis (Table 1). Ribosome footprints at the start site of an open reading frame are a good proxy for the expression of the corresponding protein. However, it is critical to establish whether a given small open reading frame (sORF) results in a protein product of that specific size. All but one protein YoaI were previously validated for expression via genomic epitope-tagging (Table S5). In the case of YoaI, the protein could not be detected in rich media or specific growth conditions, including envelope stress, acid stress, and heat shock (Hemm *et al*, 2008, 2010). Given the strong signal for expression of YoaI in our Ribo-RET data (~12-fold increase in RPM for stress vs. no stress) (Fig. S4A), we wondered if YoaI is conditionally expressed during magnesium limitation. To examine the expression of YoaI, we utilized a strain carrying chromosomally-encoded fusion protein YoaI-SPA (Hemm *et al*, 2008, 2010). We grew cells in media containing different levels of Mg^{2+}, prepared membrane and cytoplasmic fractions, and performed western blot analysis. Consistent with our hypothesis, we detected expression of YoaI in a magnesium-dependent manner, where the protein level is highest at the lowest concentration of magnesium (Fig. S4B). In addition, this result also confirms that YoaI is predominantly associated with the membranes, consistent with the bioinformatic prediction that it is a membrane protein (Table S7).

14 of the 17 shortlisted small proteins were not previously associated with expression under low magnesium stress. Small proteins YobF (Hemm *et al*, 2010; Hobbs *et al*, 2010) and DinQ (Weel-Sneve *et al*, 2013) have been linked to other stress responses in *E. coli*, here we find the expression of these two proteins in low magnesium stress as well. Many of these small proteins have not been characterized biochemically and have no documented function yet. In the following sections, we systematically study these low-Mg^{2+}-induced small proteins by investigating their transcriptional regulation and cellular localization and characterizing their overexpression and deletion phenotypes.

Transcriptional regulation of low magnesium stress-induced small proteins

To determine changes in the levels of transcripts encoding stress-induced small proteins, we performed RNA-Seq using cells grown to early exponential phase in high and low Mg^{2+} conditions. It is well-established that in cells depleted for Mg^{2+}, the PhoQP signaling system is stimulated, leading to PhoP-mediated transcriptional activation of hundreds of genes necessary for the stress response (Groisman *et al*, 2021). Not surprisingly, we see an increase in the mRNA abundances for *phoQ* and *phoP* (Fig. S3). Differential expression analysis of our RNA-seq data revealed significant upregulation (fold change threshold of >2 and a p-value threshold of <0.05) in transcription under low Mg^{2+} stress for at least 10 of the 17 small proteins shortlisted, including MgtS, MgtT, and MgrB (Fig. 2A). It is worth noting that YadX also showed a small increase (1.7-fold) although it falls below the >2-fold threshold we applied in our data analysis. Intriguingly, YriA, whose open reading frame overlaps with YriB by ~60% did not show an increase in the transcript levels. In addition, we did not see a significant change in the mRNA levels corresponding to YoaI, YobF, YkgS, and DinQ. In these cases, it is possible that the

197 change in transcript abundances is generally low and therefore fell below the significance
198 threshold. Alternatively, gene expression might be regulated at a post-transcriptional or
199 translational level under low magnesium stress. Indeed, *yobF* expression is induced post-
200 transcriptionally during heat shock response (Hemm *et al*, 2010). The expression of *yobF* under
201 magnesium limitation may be controlled via a similar post-transcriptional regulatory mechanism.

202 To delve deeper into the transcriptional control mechanism of the small proteins we sought to:
203 1) identify the regulatory regions upstream of each sORF, and 2) determine if the expression is
204 PhoQ-dependent. To identify the regions containing the putative promoters of low Mg^{2+}-induced
205 small proteins, we carefully selected ~200 to 500 base pairs upstream of each sORF (Table
206 S6). In general, we did not include any annotated full-length ORFs or non-coding RNAs
207 occurring within the regulatory region being tested, to avoid interference from the ectopic
208 expression of the corresponding product. In cases where a sORF appeared to be in the middle
209 of an operon, we selected two regions to test: one upstream of the entire operon and another
210 immediately upstream of the sORF of interest. We designed transcriptional reporter constructs
211 to measure the activity of each putative regulatory region, as shown in the schematic (Fig. 2B).
212 To analyze which of these sORFs are regulated by the PhoQP two-component system, we
213 measured the transcriptional reporter activities in a *phoQ* deletion strain and compared them to
214 that of the wild type (Fig. 2C).
215
216 Consistent with our RNA-seq data, we saw an increase in the transcriptional activity for
217 regulatory regions corresponding to 11 sORFs with this upregulation under low Mg^{2+} condition
218 being PhoQ-dependent (Fig. 2C). Two sets of overlapping (out-of-frame) sORFs including
219 *mgtS-mgtT* and *yriA-yriB*, strongly suggest their association within the same operon. Three
220 other genes, *yadW, ymiC,* and *ydgU* are likely regulated as part of the operons, *yadX-clcA-*
221 *yadW*, *ymiA-yciX-ymiC*, and *asr-ydgU*, respectively. For all the sORFs occurring within an
222 established or putative operon, the region upstream of the operon showed a higher
223 transcriptional reporter activity in response to stress, while a second region immediately
224 upstream of the given sORF had negligible activity (Table S6, Fig. 2C). Based on the reporter
225 assay, the transcriptional activity for the 11 sORFs (*mgrB*, *mgtS*, *mgtT*, *ymiA*, *ymiC*, *yddY*, *yriA*,
226 *yriB, yadX*, *yadW*, and *ydgU*) peaks at ~6-10 hours. The RNA-Seq data represent
227 transcriptomic abundances at a given time point of growth (early exponential phase). This
228 transcriptional reporter assay captures temporal changes in the reporter activity and serves as a
229 complementary approach to RNA-Seq, where changes in low-abundance transcripts would be
230 missed. For instance, we did not observe a significant upregulation of *yadX* and *yadW* in the
231 RNA-Seq data, but we see a PhoQ-dependent increase in the reporter activity for the putative
232 regulatory region $P_{yadX\text{-}clcA\text{-}yadW}$ region under low magnesium stress. Conversely, for *pmrR* and
233 *yqhI*, while the RNA-Seq data suggested upregulation, we did not detect a significant increase
234 in the transcriptional reporter activity under stress suggesting that there may be distal or
235 additional regulatory factors, outside of our reporter construct, involved in controlling their
236 transcription. Indeed, *pmrR* is shown to be transcriptionally activated by the PmrA-PmrB
237 signaling system during magnesium limitation through the PhoQP-regulated connector protein
238 PmrD in *Salmonella enterica* (Kato *et al*, 2012) . This connection between the PhoQ-PhoP and
239 PmrA-PmrB signaling pathways is also active in *E. coli* under specific conditions including high

stimulation of the PhoQ-PhoP system (Chen *et al*, 2021; Rubin *et al*, 2015). We did not observe a reporter activity for *dinQ, ykgS, yobF*, and *yoaI* in either the wild-type or *ΔphoQ* cells, consistent with the results from the RNA-Seq.

In summary, our RNA-Seq and transcriptional reporter assays reveal transcriptional upregulation of 13 of the 17 small proteins, of which PhoQ regulates at least 11 under magnesium starvation.

Regulation of small membrane protein YoaI under Mg^{2+} stress

YoaI is known to be regulated by the PhoRB two-component system (Fitzgerald *et al*, 2023; Yoshida *et al*, 2012; Chekabab *et al*, 2014), which responds to phosphate starvation (Gardner & McCleary, 2019). PhoRB signaling is also activated under low magnesium stress due to the slowdown of protein synthesis and reduction of cytoplasmic phosphate levels (Pontes & Groisman, 2018). Consistently, we noticed a 10-fold increase in reads mapping to the PhoB translation start site under magnesium stress (Fig. S2D). We then tested our transcriptional reporter for *yoaI* (P_{yoaI}-YFP) in a low-phosphate medium and saw increased transcriptional activity for P_{yoaI} when compared to no-stress condition, in a PhoB-dependent manner (Fig. 3A). This transcriptional activation is PhoQ-independent as we see an amplification of P_{yoaI} reporter in Δ*phoQ* cells as well (Fig. 3B). Taken together, these results show that *yoaI* transcription is controlled by PhoB, and there is no significant effect of low magnesium stress on *yoaI* transcription based on RNA-Seq and transcriptional reporter data (Fig. 2A, C). Yet YoaI protein levels increase under low magnesium conditions, and we wondered if PhoQ controls YoaI abundance. To test this possibility, we examined YoaI protein expression in wild-type and Δ*phoQ* cells in high and low magnesium conditions by western blotting. Our results demonstrate that YoaI's expression remains magnesium-dependent in a Δ*phoQ* strain, mirroring the pattern seen in the wild type (Fig. 3C), suggesting that PhoQ does not affect YoaI levels. Therefore, YoaI expression is induced in a PhoQ-independent manner under magnesium limitation potentially via a post-transcriptional regulatory mechanism that enhances translation initiation.

About half of the low Mg^{2+} stress-induced small proteins localize to the membrane

As a first step to classifying the 17 stress-induced small proteins, we checked if a given small protein is likely associated with the membrane or cytoplasm. Most of these proteins have limited or no documented information, so their cellular localization can provide insights into their potential mechanisms of action and interactions within the cell. Using bioinformatic tools TMHMM (Möller *et al*, 2001), TMPred (Ikeda *et al*, 2003), and Phobius (Käll *et al*, 2004) to predict membrane helices, we find that at least 9 of our candidates are putative membrane proteins. Three of them, MgrB, MgtS, and DinQ, were previously shown to localize to the membrane in *E. coli* (Hemm *et al*, 2008; Weel-Sneve *et al*, 2013). Additionally, PmrR from *S. enterica* was shown to be membrane-bound (Kato *et al*, 2012). Our bioinformatic analyses predict that small proteins YdgU, YmiA, YmiC, YoaI, and YobF also localize to the membrane (Table S7).

Next, to confirm the membrane association and visualize the small protein localization we used epitope-tagging with GFP. Taking into account the predicted orientation of the putative

284 transmembrane protein, we created either an N- or C-terminal fusion of GFP by tagging the end
285 that is expected to face the cytoplasm (Fig. S5A, Table S7) to ensure proper folding of GFP
286 (Feilmeier *et al*, 2000). Accordingly, YdgU, YmiA, and YmiC were tagged at the N-terminus, and
287 YoaI was tagged at the C-terminus. Upon observation by fluorescence microscopy, cells
288 expressing GFP-tagged YdgU, YmiA, YmiC, and YoaI revealed bright fluorescence at the cell
289 periphery indicative of membrane localization, similar to the known membrane protein, MgrB
290 (Fig. S5B). As a control, cells expressing GFP alone showed uniform fluorescence indicative of
291 cytoplasmic localization.
292
293 For PmrR, we constructed an N-terminal fusion with GFP, where the tag was expected to
294 localize to the cytoplasm. However, we did not observe membrane localization (Fig. S5B).
295 Considering the predicted membrane helices, this suggests that the tag interferes with PmrR
296 localization. Alternately, we tagged the C-terminus of *E. coli* PmrR with a hexahistidine (6XHis)
297 tag (Fig. S5C) and performed western blotting using membrane and cytoplasmic fractions.
298 PmrR-6XHis strongly associated with the membrane fraction (Fig. S5D), consistent with the
299 bioinformatic prediction and data from *S. enterica* PmrR. As in the case of PmrR, YobF-GFP
300 localized to the cytoplasm, which was inconsistent with its predicted membrane localization
301 (Table S7). Therefore, we used a 6XHis-tagged version of YobF, which showed a greater
302 association with the membranes than the cytoplasmic fraction (Fig. S5D). Overall, among the 17
303 small proteins induced under low Mg^{2+}, we find that 9 of them are membrane proteins.
304

305 **Three small proteins exhibit stress-specific growth defects upon gene deletion**

306 To identify potential defects in growth and cellular morphology caused by the absence of each
307 small protein in the cell, we utilized single gene deletions of *mgtS*, *mgtT*, *pmrR*, *yadW*, *yadX*,
308 *yddY*, *ykgS*, *ymiC*, *yqhI*, *yobF, dinQ*, *ydgU*, *ymiA*, and *yoaI* in the *E. coli* genome. *mgtT* lies in an
309 operon with *mgtS* (Weaver *et al*, 2019), with an out-of-frame overlap between the stop codon of
310 MgtS and the start codon of MgtT. Therefore, we carefully generated an *mgtS* deletion without
311 affecting the start codon of MgtT, and similarly, an *mgtT* deletion while keeping the stop codon
312 for MgtS intact (for details see materials and methods, Table SI). In the case of *yriAB*, the two
313 small proteins YriA and YriB have overlapping open reading frames, where ~80% of the *yriB* gene
314 overlaps with that of *yriA* (Fig. 4D, schematic), so, we first deleted the combined *yriAB* ORF to
315 see if there is a phenotype. 12 out of the 17 small proteins displayed no discernible growth defects
316 upon deletion relative to the wild-type strain when grown under magnesium limitation. However,
317 four mutants – namely *ΔpmrR, ΔyobF, ΔyqhI,* and *ΔyriAB* – exhibit reduced growth yields when
318 grown over 24 hours (Fig. 4A). The cells carrying these deletions entered the stationary phase
319 earlier than the wild type. Notably, PmrR and YobF are membrane-bound proteins, while YqhI,
320 YriA, and YriB are putative soluble proteins (Fig. S5D, Table S7).
321
322 To determine whether these growth defects are specifically related to the loss of these small
323 proteins, we complemented the deletion strains with plasmids encoding the corresponding small
324 proteins and induced with IPTG. Successful rescue of growth is observed for *ΔpmrR*, and *ΔyobF*
325 (Fig. 4B-C; top panel). To confirm that this complementation is specific to the small protein and
326 not due to a cryptic ORF or regulatory element present within the small protein coding region, we
327 prepared plasmids carrying *pmrR* and *yobF* where their start codons are mutated to stop codons.

328 When tested for complementation in *ΔpmrR* and *ΔyobF*, respectively, the start codon mutants
329 retained the growth defect similar to that observed for the empty vector (Fig. 4B-C; top panel),
330 reinforcing that the growth phenotype is specific to the small proteins themselves. In addition, we
331 investigated whether the growth defect observed with *pmrR* and *yobF* deletions is specific to low
332 magnesium stress. Our results indicate that deletions of *pmrR* and *yobF* do not cause growth
333 defects in the absence of stress (Fig. 4B-C; bottom panel), and the phenotype is specific to
334 magnesium-limited conditions. Intriguingly, expression of plasmid-encoded PmrR in the absence
335 of stress resulted in a growth defect (Fig. 4B, bottom panel), suggesting that increased expression
336 of PmrR under no-stress conditions may be detrimental.
337
338 Given the growth phenotype observed for Δ*yriAB*, we performed complementation with either
339 plasmid-encoded YriA and/or YriB to establish if the loss of either protein is responsible for the
340 growth defect. Intriguingly, complementation with either YriA or YriB alone failed to restore growth
341 but a plasmid expressing the region from *yriB* to *yriA,* mimicking the native genomic arrangement
342 (*yriAB*), partially rescued the growth defect (Fig. 4D, top panel). In our plasmid construct encoding
343 YriB and YriAB, there is a possibility of a spurious small protein produced due to the intact, out-
344 of-frame YriA start codon within the *yriB* ORF (Fig. 4D, schematic) that potentially interferes with
345 the complementation. To address this issue, we created a modified *yriB* construct where YriA
346 start codon ATG is mutated to TAA, this substitution changes codons 4 (Asp) and 5 (Val) in YriB
347 to 4 (Ile) and 5 (Ile). This variant of YriB confers full complementation (Fig. 4D, top panel),
348 indicating that loss of YriB contributes to the growth phenotype, at least in part. In addition, we
349 see that the growth defect associated with *yriAB* deletion is specific to low magnesium stress
350 condition (Fig. 4D, bottom panel).
351
352 Finally, the growth defect observed in *ΔyqhI* is not complemented with a plasmid encoding YqhI
353 (Fig. 4E), which suggests that this phenotype is not directly related to the YqhI protein itself.
354 Intriguingly, we did not see a growth defect in *ΔmgtS* strain when grown in a low magnesium
355 medium (Fig. 4A), contrasting with the previous report (Wang *et al*, 2017). This discrepancy might
356 be due to differences in strain construction and/or growth media. Together, our results underscore
357 the complexities in studying overlapping small ORFs and their phenotypes.
358

359 **Seven small proteins affect growth and cell morphology upon overexpression**

360 As a parallel approach to analyzing loss-of-function phenotypes, we explored the phenotypes
361 associated with the overexpression of small proteins. We cloned the genes corresponding to the
362 untagged small proteins into either an IPTG-inducible (all except DinQ as we were unable to
363 generate a DinQ clone in the IPTG-inducible pEB52 background) or arabinose-inducible (DinQ)
364 vector. Upon induction, slow growth or a prolonged lag phase is observed for 7 out of the 17 small
365 proteins tested: MgtS, MgrB, PmrR, YmiA, YoaI, YkgS, and DinQ (Fig. 5). Notably, six of these
366 proteins are membrane-bound (MgtS, MgrB, PmrR, YmiA, YoaI, and DinQ). In the case of MgtS,
367 MgrB, PmrR, YmiA, and YoaI, induction of expression with IPTG leads to an extended lag phase
368 lasting for ~8-10 hours, after which the cells grow exponentially at growth rates similar to that of
369 control cells carrying empty vector, eventually reaching saturation at comparable levels.
370 Interestingly, cells expressing small proteins YkgS and DinQ did not display a long lag phase but
371 grew at a slower rate, eventually catching up to the same growth yield as the control cells. The

372 growth defect due to DinQ overexpression aligns with previous studies indicating that its
373 overexpression disrupts membrane potential and depletes intracellular ATP levels (Weel-Sneve
374 *et al*, 2013). It is worth noting that overexpression of the other 10 small proteins, including 3
375 membrane proteins YdgU, YmiC, and YobF had a negligible impact on cell growth under the same
376 condition, suggesting that cells may tolerate high amounts of these proteins (Fig. 5). More
377 importantly, the lack of a phenotype for most of these small proteins indicates that the growth
378 defects observed here are not due to a generic burden on the cell from plasmid-driven protein
379 overexpression.
380
381 To be cautious in interpreting the overexpression data, we considered the possibility that the
382 observed growth defects might be attributed to a cryptic small open reading frame or regulatory
383 element within the small ORF being overexpressed. To check if the growth defects are indeed
384 small protein-dependent, we prepared plasmid constructs containing variants of the small protein
385 where the start codon (ATG) is substituted with a stop codon (TAA). For all 7 small proteins
386 displaying overexpression phenotypes, we repeated the growth assay with the start codon
387 mutants of each small protein. Expression of the mutant small proteins rescued the growth defect
388 with the cells exhibiting similar growth patterns to those carrying the empty vector (Fig. 6A),
389 reinforcing that the observed growth defects are specific to the overexpression of these small
390 proteins.
391
392 In addition to the impact on growth, we explored whether overexpression of these 7 small proteins
393 (MgtS, MgrB, PmrR, YmiA, YoaI, YkgS, and DinQ) influences cell size and morphology, especially
394 given the delayed growth (Fig. 5, 6A). We hypothesized that cells overexpressing these small
395 proteins may undergo morphological changes as part of adaptation during the extended lag and
396 log phases of growth. Using phase contrast microscopy, we imaged cells induced for expression
397 of the small proteins during the lag and exponential growth phases. As controls, we used wild-
398 type cells carrying either an empty vector or a plasmid containing a variant of the small ORF
399 where its start codon (ATG) is mutated to a stop (TAA). The control cells exhibited a roughly
400 uniform cell size with volumes around 1.1-1.3 fL and 1.2-1.4 fL in lag and log phases, respectively.
401 Intriguingly, overexpression of small proteins MgtS, MgrB, PmrR, YkgS, YoaI, and YmiA causes
402 distinct changes in cell size (Fig. 6B, S6). Specifically, overexpression of MgtS results in smaller
403 cell size (Fig. 6B), with a reduction in cellular volume to ~30-36% of the control cells carrying
404 either empty vector or start codon mutants in both lag and log phases (Fig. S6). Similarly,
405 overexpression of PmrR and YoaI leads to a ~29% decrease in cell size and volume during the
406 lag phase, however, the cell size reverts to that of control cells during the exponential phase (Fig.
407 6B, S6). In contrast, overexpression of MgrB leads to an increase in cell size, with an average
408 volume of 2.2 fL, ~1.6-fold larger than the controls in the lag phase (Fig. 6B, S6), akin to the
409 Δ*phoQ* cells grown in low magnesium conditions (Fig. S7). This finding is remarkable because
410 MgrB is known to inhibit PhoQ (Lippa & Goulian, 2009; Yadavalli Srujana S. *et al*, 2020),
411 consistently, plasmid overexpression of MgrB likely leads to strong inhibition of PhoQ, resulting
412 in a cellular morphology similar to that of Δ*phoQ*. These cells eventually return to normal size (cell
413 volume of 1.2 fL) in the exponential phase. Overexpression of YkgS and YmiA causes varying
414 extents of cell elongation affecting cell size and volume (Fig. 6B, S6). Cells overexpressing DinQ
415 did not show a significant change in cell size.

416
417 Overall, the slow or delayed growth observed here along with the diverse morphological
418 phenotypes at distinct growth stages reflects how cells adapt in response to the overexpression
419 of small proteins mentioned above.
420

421 **Small protein YoaI connects distinct signaling systems – PhoQ-PhoP, PhoR-PhoB, and**
422 **EnvZ-OmpR**

423 We wondered whether the growth delay observed upon overexpression of the 7 small proteins
424 described above is PhoQ-dependent, given the pivotal role of PhoQ in low magnesium stress. To
425 explore this, we evaluated the effects of overexpressing these proteins in a Δ*phoQ* strain under
426 magnesium limitation. Notably, the growth phenotype associated with protein overexpression is
427 retained in the Δ*phoQ* cells, similar to those observed in the wild-type strain for 6 out of 7
428 candidates – MgrB, MgtS, PmrR, YmiA, YkgS, and DinQ (Fig. 6C), indicating that these effects
429 are PhoQ-independent. Interestingly, in the case of YoaI overexpression, the extended lag phase
430 observed in wild-type cells is completely abolished in the Δ*phoQ* cells, suggesting a direct or
431 indirect link between PhoQ and YoaI where PhoQ functions upstream of YoaI in this regulatory
432 pathway.
433

434 To check if YoaI and PhoQ physically interact with each other, we employed a bacterial two-hybrid
435 (BACTH) assay based on reconstituting split adenylyl cyclase (CyaA) (Battesti & Bouveret, 2012;
436 Karimova *et al*, 1998). In this system, CyaA activity is restored when the two fragments T18 and
437 T25 come close leading to an increase in cyclic AMP (cAMP) levels and subsequent expression
438 of β-galactosidase (β-gal) from the *lac* promoter. We fused the T18 fragment to YoaI and tested
439 it against T25-PhoQ. We included the T18-MgrB and T25-PhoQ pair as a positive control and two
440 other histidine kinases, PhoR and EnvZ, each fused to the T25 fragment as additional controls.
441 In this experiment, YoaI did not show an interaction with either PhoQ or PhoR, however, to our
442 surprise there was a strong signal between YoaI and EnvZ that is comparable to the positive
443 control (Fig. 7A). EnvZ is primarily known to be an osmosensor, integral to the EnvZ-OmpR two-
444 component system, which regulates porins in response to changes in osmolarity, pH,
445 temperature, and growth phase (Kenney & Anand, 2020). Several small membrane proteins are
446 known to modulate the activities of sensor kinases (Yadavalli & Yuan, 2022). A 127-amino acid
447 protein, MzrA regulates EnvZ resulting in higher levels of phosphorylated OmpR (Gerken *et al*,
448 2009). Based on the BACTH interaction between YoaI and EnvZ, we suspected YoaI might
449 influence the activity of the EnvZ-OmpR signaling system. To address this possibility, we utilized
450 an EnvZ-OmpR-regulated transcriptional reporter strain with chromosomal fusion of mScarlet to
451 P_{omrB} (Bastet *et al*, 2024) and measured *omrB* promoter activity in cells grown in low magnesium
452 vs. no-stress media. Interestingly, we observe an increase of 2.5-fold in EnvZ-regulated
453 transcription under stress in wild-type cells (Fig. 7B). The significantly high activity of *omrB*
454 reporter in low Mg^{2+} conditions suggests that upregulation of YoaI protein levels may mediate this
455 effect (Fig. 3C, S4). Upon deletion of *yoaI*, the *omrB* transcription reduced by ~1.4-1.5-fold in both
456 low and high Mg^{2+} media, indicating that YoaI affects EnvZ-OmpR activity regardless of stress.
457 Together with our observation that YoaI-SPA levels increase under low Mg^{2+} stress (Fig. 3C,
458 S4B), the higher transcriptional activity of the EnvZ-regulated promoter can be attributed to the
459 positive interaction of YoaI with EnvZ. To further support the idea that an increase in YoaI levels

is responsible for modulating the activity of the EnvZ-OmpR system, we examined *omrB* transcription upon plasmid overexpression of YoaI in wild-type *E. coli* cells. We observed a greater than 6-fold increase in P_{omrB}-*lacZ* reporter activity in cells expressing YoaI on a plasmid (Fig. S8A) relative to the control cells carrying an empty vector. We also tested two other reporters to genes *ompF*, P_{ompF}-YFP and *ompC*, P_{ompC}-CFP (Batchelor *et al*, 2004), and found a ~2-fold change in their transcriptional activities (Fig. S8B-C), consistent with the activation of EnvZ (Alphen & Lugtenberg, 1977; Batchelor *et al*, 2005; Kenney & Anand, 2020). In summary, these findings suggest that YoaI interacts with and stimulates EnvZ activity, potentially enhancing OmpR-P levels.

Discussion

In this study, we identified 17 small proteins (≤50 amino acids) induced by low magnesium stress from approximately 150 documented small proteins in *E. coli*, using Ribo-RET (Meydan *et al*, 2019; Weaver *et al*, 2019). Only 3 of these proteins, MgrB, MgtS, and PmrR were previously studied in the context of magnesium starvation (Lippa & Goulian, 2009; Wang *et al*, 2017; Kato *et al*, 2012). For all the stress-induced small proteins except one (YoaI), expression from the genomic locus was verified *in vivo* (Table S5). In a previous report when cells were grown in a rich medium, expression of YoaI tagged with SPA epitope from a genomic translation fusion was undetected (Hemm *et al*, 2008). Interestingly, our observation of cells grown in low Mg^{2+} detected a robust expression of YoaI expression using the same construct, highlighting the condition-specific expression of this protein (Fig. 3C, S4B). Using RNA-Seq, we found that many of these stress-induced proteins are transcriptionally activated in low magnesium media. Further, we identified the regions upstream of these small ORFs responsible for transcriptional regulation using operon fusions and reporter assays. Few hits, including YoaI and YobF, do not show a change in transcription levels under low Mg^{2+}, suggesting that they are regulated post-transcriptionally.

Lacking any functional or phenotypic information for most of these stress-induced proteins, we began their characterization by predicting their subcellular localization using bioinformatic tools (Tables 1, S7). By epitope tagging and imaging or western blotting, we empirically determined that 9 of the 17 shortlisted stress-induced small proteins localize to the membrane (Fig. S5). These membrane-bound small proteins may interact with, stabilize, or fine-tune the activities of large transmembrane proteins, such as sensor kinases, channel proteins, and drug efflux pumps, thereby mediating cellular adaptation and stress responses (Yadavalli & Yuan, 2022). Among the 9 candidates, three proteins – MgrB, MgtS, and PmrR are shown to have specific membrane protein targets, as described earlier. To further investigate their biological roles, we performed targeted deletion and protein overexpression analysis.

Loss-of-function analysis of small proteins can be a useful approach to understanding their physiological roles. For example, deleting *mgrB* causes hyperactivation of the PhoQP two-component system, leading to cell division inhibition and filamentation of cells grown under low magnesium stress (Yadavalli *et al*, 2016). In clinical isolates of *Klebsiella pneumoniae,* the absence of MgrB-mediated PhoQ inhibition has been linked to acquired colistin resistance

504 (Cannatelli *et al*, 2014; Olaitan *et al*, 2014). In the current work, we found deletion phenotypes
505 associated with the following small proteins—PmrR, YobF, YriA/B, and YqhI—leading to an early
506 entry into the stationary phase and reduced yield at saturation under magnesium limitation. Based
507 on plasmid complementation, growth defects caused by PmrR and YobF are specific to the
508 respective small proteins. The overlapping ORFs of YriA and YriB present a unique challenge in
509 interpreting the Δ*yriAB* growth phenotype observed under low magnesium stress. While
510 expressing the native *yriAB* region partially rescues the defect, individual expression of YriA or
511 YriB fails to do so; however, modifying YriB by mutating the out-of-frame YriA start codon fully
512 restores growth, emphasizing that the loss of YriB is a critical factor in the observed phenotype.
513 In the case of YqhI, the deletion phenotype could not be fully complemented by plasmid-encoded
514 small protein, pointing to putative cryptic ORF or regulatory factors within the small ORF that
515 warrant further investigation.
516
517 We also analyzed overexpression phenotypes associated with each of the stress-induced small
518 proteins to gain insights into cellular pathways or components functionally linked to these proteins.
519 For instance, overexpression of MgtS is shown to activate the PhoRB two-component system by
520 regulating the phosphate transporter, PitA (Yin *et al*, 2019). Similarly, DinQ overexpression
521 disrupts membrane potential and depletes intracellular ATP levels (Weel-Sneve *et al*, 2013). We
522 observed overexpression phenotypes for 7 of the 17 small proteins induced under magnesium
523 stress—MgtS, MgrB, PmrR, YmiA, YoaI, YkgS, and DinQ—resulting in either a long lag phase or
524 slow growth (Fig. 5). These overexpression phenotypes are specific to each small protein as we
525 see control plasmids carrying a mutated start codon do not cause growth defects (Fig. 6A).
526 Analysis of the cell morphology during the lag and exponential phases of growth revealed
527 interesting variations in cell sizes and volumes that reflect how cells adapt to the overexpression
528 of these small proteins. Remarkably for one of the small proteins, PmrR, both the deletion and
529 overexpression caused growth defects under low magnesium stress. It is unclear how cells
530 balance small protein levels when needed during specific conditions vs. when not needed, say in
531 the absence of stress. In this context, complementation of the *ΔpmrR* strain with plasmid-encoded
532 PmrR restored normal growth under magnesium limitation but caused a growth defect under no-
533 stress condition (Fig. 4B). This suggests that PmrR levels may be controlled precisely in cells
534 undergoing stress, as both its absence and its overexpression disrupt the balance necessary for
535 cellular homeostasis.
536
537 In *Salmonella enterica,* PmrR has been shown to inhibit the inner membrane protein LpxT, which
538 plays a role in lipopolysaccharide modification (Kato *et al*, 2012; Tian *et al*, 2021; Hong *et al*,
539 2018). We explored whether the growth defects associated with PmrR deletion and
540 overexpression in *E. coli* are mediated through its interaction with LpxT. Interestingly, expressing
541 PmrR in a Δ*lpxT* background did not alleviate the growth defects regardless of stress (Fig. S9A).
542 It is possible that higher LpxT levels, resulting from the absence of PmrR, could lead to growth
543 defects. However, both single deletions (*ΔlpxT* and *ΔpmrR*) and the double deletion (*ΔpmrR*
544 *ΔlpxT*) exhibited growth defects under magnesium stress (Fig. S9B). This result suggests that the
545 growth defect upon *pmrR* deletion is independent of PmrR's interaction with LpxT. PmrR may be
546 involved in other pathways or regulatory mechanisms where it has additional interacting partners.
547 It is not uncommon for small proteins to have multiple binding partners, as seen with MgtS, which

548 interacts with both MgtA and PitA (Yin *et al*, 2019; Wang *et al*, 2017). Whether PmrR associates
549 with other targets contributing to phenotypes observed here warrants further investigation.
550
551 Finally, we would like to discuss the interesting case of the small membrane protein YoaI,
552 whose transcription is controlled by the PhoR-PhoB signaling system (Fitzgerald *et al*, 2023;
553 Yoshida *et al*, 2012; Chekabab *et al*, 2014). YoaI levels are quite low or undetectable when cells
554 are grown in a rich medium or specific stress conditions (Hemm *et al*, 2008, 2010). However, we
555 find that YoaI protein levels strongly increase under magnesium limitation and it becomes
556 detectable (Fig. 3C). Overexpression of YoaI leads to a long delay in growth (Fig. 5, 6A, S4B).
557 This phenotype is abolished in a *phoQ* mutant (Fig. 6C), hinting at an unknown PhoQ-
558 dependent factor that may contribute to the growth defect observed upon YoaI overexpression.
559 Through a bacterial two-hybrid assay, we found a direct interaction of YoaI with the EnvZ sensor
560 kinase (Fig. 7A), which controls osmoregulation (Kenney & Anand, 2020) suggesting that this
561 small protein acts as a connector between the PhoR-PhoB and EnvZ-OmpR signaling networks.
562 Activation of EnvZ by YoaI is supported by the data from our transcriptional reporter analysis of
563 promoters regulated by the EnvZ-OmpR system (Fig. 7B, S8). Modulation of sensor kinases via
564 small protein connectors appears to be a general theme that many small membrane proteins of
565 unknown function may fall under (Yadavalli & Yuan, 2022). For instance, under acidic
566 conditions, a 65-amino acid protein SafA is activated by the EvgS-EvgA two-component system,
567 which subsequently interacts with and activates the PhoQ-PhoP system (Eguchi *et al*, 2007). In
568 a second example, an 88-amino acid protein PmrD connects the PmrB-PmrA and PhoQ-PhoP
569 signaling systems in *Salmonella* (Kox *et al*, 2000; Kato & Groisman, 2004). Another 127-amino
570 acid protein MzrA is known to bind and activate EnvZ, which links the CpxA-CpxR and EnvZ-
571 OmpR pathways in *E. coli* (Gerken *et al*, 2009). Taken together, our findings outlining the
572 transcriptional regulation of YoaI by PhoB (Fig. 3A), PhoQ-dependent growth phenotype upon
573 YoaI overexpression (Fig. 6C), and YoaI's physical interaction with EnvZ and modulation of
574 EnvZ-regulated promoter activity (Fig. 7B, S8) reveal how this 34-amino acid small protein acts
575 as a connector between distinct two-component signaling systems – PhoRB, PhoQP, and EnvZ-
576 OmpR to integrate diverse stress responses (Fig. 7C).
577
578 Most small proteins (≤50 amino acids in prokaryotes) are of unknown function and little is known
579 about when/if they are expressed in the cell and what their physiological relevance is. Small
580 proteins are thought to fine-tune the activity and/or stability of larger target molecules in the cell,
581 adding a layer of gene regulation. This type of conditional regulation by small proteins may be
582 especially important when cells are grown in non-ideal or stressful environments. Overall, our
583 work describing the identification of condition-specific small proteins and targeted phenotypic
584 characterization provides a deeper understanding of small protein regulation and the
585 physiological consequences of altering their expression levels, laying a foundation for
586 deciphering their functions and regulatory mechanisms under relevant stress conditions.
587
588
589

590 # Methods
591
592 **Media and growth conditions**
593 Bacterial cultures were grown in either Luria-Bertani (LB) Miller medium (IBI Scientific) or
594 minimal A medium (Miller & Others, 1992) supplemented with 0.2% glucose, 0.1% casamino
595 acids, and the indicated concentration of $MgSO_4$, with aeration at 37°C, unless otherwise
596 specified. In general, overnight cultures are grown in supplemented minimal A medium
597 containing 1 mM $MgSO_4$ and antibiotic(s) as applicable. Saturated cultures are diluted 1:500 into
598 fresh medium. For low Mg^{2+} stress, no Mg^{2+} was added when overnight cultures were diluted
599 into fresh medium. Media containing 10 mM Mg^{2+} was used as the no-stress condition. For
600 phosphate stress experiments, MOPS minimal medium (Teknova) supplemented with 0.2%
601 glucose, 0.1% casamino acids, and either 1 mM K_2HPO_4 (no-stress) or no K_2HPO_4 (phosphate
602 stress). For routine growth on solid medium, LB containing 1.5% bacteriological-grade agar
603 (VWR Lifesciences) was used. For antibiotic selection, carbenicillin, kanamycin, and
604 chloramphenicol were added at a final concentration of 50-100 µg ml^{-1}, 25- 50 µg ml^{-1}, and 6-25
605 µg ml^{-1}. b-isopropyl-D-thiogalactoside (IPTG) was used at a final concentration of 500 µM,
606 unless otherwise specified. Arabinose was used at final concentrations of 0.5% and 30 mM for
607 pBAD24-based vectors and pMR120-based vectors, respectively, to induce protein expression
608 when needed.
609
610 **Strains, plasmids, and cloning**
611 See supplemental information for details of the strains (Table S1), plasmids (Table S2), and
612 primers (Table S3) used in this study. All the strains used were derived from *Escherichia coli K-*
613 *12* MG1655. Strain JW2162 was a gift from Dr. Bryce Nickels; plasmids pEB52, pAL38, pAL39,
614 pSMART, pMR120 and strains AML67, MDG147, TIM92, TIM100, and TIM202 were gifts from
615 Dr. Mark Goulian. Strains GSO195, GSO219, GSO225, GSO232, and GSO317 were gifts from
616 Dr. Gisela Storz. Strains JM2110 and JM2113 were kind gifts from Dr. Maude Guillier.
617
618 A modified version of the method described by (Datsenko & Wanner, 2000) was used to
619 generate in-frame gene deletions corresponding to each small protein. Briefly, the entire small
620 open reading frame (sORF) (including the stop codon) was deleted from the MG1655 genome
621 and substituted with a kanamycin resistance cassette. While constructing the gene deletions,
622 we avoided deleting any overlapping annotated ORFs, non-coding RNAs, or putative regulatory
623 regions in the vicinity of the target gene. In the case of *yriA-yriB (yriAB),* the two small protein
624 ORFs significantly overlapped; therefore, we deleted the combined *yriAB* ORF. Detailed
625 information on the genomic coordinates of deleted regions can be found in Table S1. Genomic
626 deletions and reporter constructs carrying the kanamycin resistance cassettes were transferred
627 between strains using $P1_{vir}$ transduction (Miller & Others, 1992) and validated by PCR. When
628 necessary, the kanamycin cassette was excised from the chromosome by FLP-mediated
629 recombination using pCP20, as previously described (Cherepanov & Wackernagel, 1995). PCR
630 and loss of antibiotic resistance confirmed the excision of the kanamycin cassette.
631
632 Plasmids expressing translational fusions of GFP-A206K to the small open reading frames
633 (sORFs), specifically pPJ1-13 and pSV25, were generated through inverse PCR (Ochman *et al*,

634 1990) using pAL39 as a template. Plasmids encoding C-terminally 6XHis-tagged-YobF and -
635 PmrR (sORF-GGSG linker-6XHis) were created using inverse PCR with pEB52 as a template,
636 resulting in pSV14 and pSV26, respectively. Plasmids encoding untagged small proteins
637 (pSV30-pSV37, pSV58, pSV60, and pJS1-pJS7) were also generated by inverse PCR with
638 pEB52 as a template. pSV54 was generated by inverse PCR using pBAD24 as a template.
639 Plasmids pSV38-pSV45, pSV55, pSV59, and pSV61, encoding variants of sORFs with start
640 codon substitutions to stop codons (TAA), were generated by site-directed mutagenesis with
641 inverse PCR using templates pSV35, pSV34, pJS7, pJS4, pSV36, pJS5, pSV54, pSV37, and
642 pSV60 as applicable. For pSV39-pSV42, another in-frame start codon within five amino acids of
643 the annotated start was also substituted to TAA. All constructs were verified by Sanger
644 sequencing. To generate pSV47, *yoaI* was PCR amplified from the MG1655 genome, digested
645 with *XbaI/EcoRI* restriction enzymes, and then cloned into pUT18C at *XbaI/EcoRI* sites.
646
647 To examine the transcriptional regulation of the sORFs and identify the putative regulatory
648 regions, ~200-500 bp upstream region of the start codon of each sORF was selected for cloning
649 (see details in Table S6). If a given sORF was suspected to be part of an operon, two putative
650 regions were chosen for analysis, the first directly upstream of the gene and a second region
651 upstream of the entire operon. Each DNA segment was amplified from MG1655 genomic DNA
652 by PCR and inserted upstream of the *yfp* reporter gene in pMR120 into the restriction sites
653 (*XhoI/BamHI* to construct pSV16, while *EcoRI-BamHI* sites were used for the remaining
654 constructs). The pMR120 vector also includes a *cfp* reporter regulated by a constitutive *tetA*
655 promoter, serving as an internal plasmid control. The resulting plasmids (pPJ14, pPJ16-pPJ20,
656 pPJ23, pSV16-21, pSV24, pSV28, pSV29) were confirmed by Sanger sequencing and
657 transformed into MG1655 and TIM202 (*ΔphoQ)*. Note that pSMART (Lucigen), pMR120, and
658 the derivatives are single-copy plasmids when transformed into *E. coli* (Godiska R, Patterson M,
659 Schoenfeld T, and Mead DA, 2005). *E. cloni* replicator cells (Lucigen) are transformed with
660 these plasmids and cultured with arabinose induction to increase the copy number for plasmid
661 isolation.
662
663 **Translation initiation profiling (Ribo-RET) and RNA-Seq**
664 Overnight cultures of wild-type *E. coli* grown in supplemented minimal A medium and 1 mM
665 $MgSO_4$ were diluted 1:500 in 100 ml of fresh medium and the specified concentrations of
666 $MgSO_4$. Once the cultures reached an OD600 of ~0.4, they were split into two 50 ml conical
667 tubes. Cells from one tube were pelleted and submitted to Genewiz for RNA-Seq, while the cells
668 from the second tube were used for Ribo-RET. For Ribo-RET, cells were treated with
669 retapamulin at a final concentration of 100 µg ml^{-1} for 5 minutes at 37°C with continuous
670 shaking. After retapamulin treatment, cells were filtered through a nitrocellulose membrane with
671 a pore size of 0.45 µm, quickly scraped off the surface, and flash-frozen in liquid nitrogen. The
672 resulting samples were processed, and libraries were prepared as described previously (Cope
673 *et al*, 2022) with the following modifications. Specifically, RNA fragments of 15-30 nucleotides
674 (nt) in length were isolated by performing a tight gel size selection, and rRNA depletion was
675 performed using the RiboCop for Gram-negative bacteria kit (Lexogen). The resulting RNA
676 fragments were then pooled, and libraries were prepared, with a final library structure consisting
677 of a 5' adapter – 4 random bases – insert – 5 random bases – sample barcode – 3' adapter. The

678 randomized bases serve as Unique Molecular Identifiers (UMIs) for deduplication. The
679 multiplexed library was sequenced on an Illumina HiSeq 4000 with a paired end reading of 150
680 bases (PE150 runs) at a sequencing depth of 40-60 million raw reads per sample.
681
682 **Sequencing data analysis**
683 The raw sequencing data for this project has been deposited in the GEO database with the
684 accession number GSE276379. An R package with codes for data processing and analysis has
685 been made available on GitHub (https://github.com/yadavalli-lab/Small-proteins-induced-under-
686 low-magnesium-stress-in-E.coli). The raw sequencing data was first demultiplexed, and the
687 adaptors were removed using cutadapt (Martin, 2011). The reads were then depleted of rRNA
688 and tRNA and deduplicated using umi_tools dedup (Smith *et al*, 2017). The Ribo-RET reads
689 were aligned to the *E. coli* MG1655 genome NC_000913.3 (RefSeq assembly accession:
690 GCF_000005845.2) using hisat2 (Kim *et al*, 2019), and the ribosome density was assigned to
691 the 3' end of the reads. Initiation peak density was calculated for the annotated translation start
692 sites by summing up the normalized reads (reads per million, RPM) within 4 to 20 nt
693 downstream of the first nucleotide in the start codon. For transcript quantification of RNA-Seq
694 reads, Kallisto (Bray *et al*, 2016) was used. DESeq2 (Love *et al*, 2014) was used for the
695 differential expression analysis of gene expression in the RNA-Seq data. Normalization of the
696 data for differential expression was carried out using the "apeglm" method (Zhu *et al*, 2019).
697 Fold-changes were estimated by comparing two replicates of the low Mg^{2+} dataset to two
698 replicates of the no-stress dataset, with filtering criteria set at more than two-fold changes and a
699 p-value below 0.05.
700
701 **Measurement of growth (optical density) and fluorescence using a microplate reader**
702 The optical density (OD_{600}) measurements for small protein overexpression and deletion
703 constructs were performed in a clear flat bottom 96-well microplate (Corning) containing 150 µL
704 culture per well using a microplate reader (Agilent BioTek Synergy Neo2S). Fluorescence
705 measurements for transcriptional reporters were carried out similarly, using black-walled, clear-
706 flat bottom 96-well microplates (Corning). Saturated cultures grown in supplemented minimal A
707 or MOPS minimal medium were normalized to the same initial OD_{600} values across all samples
708 and diluted 1:50 in fresh medium containing specified concentrations of $MgSO_4$ or K_2HPO_4,
709 along with appropriate antibiotics and inducers, as indicated. The microplates were incubated at
710 37 °C with double orbital shaking before the real-time measurements of optical density (at 600
711 nm), YFP (excitation: 500 nm; emission: 540 nm), or CFP (excitation: 420 nm; emission: 485
712 nm) were acquired every hour for 20-24 hours.
713
714 **Microscopy, and image analysis**
715 For localization of GFP-tagged small proteins, cells were grown to an OD_{600} of ~0.2 (~3 hours)
716 and then rapidly cooled in an ice slurry. Streptomycin was added to a final concentration of 250
717 µg ml^{-1}. GFP fluorescence was captured with a 475 nm excitation wavelength and a 540 nm
718 emission filter, with an exposure time of 30 ms and 20% intensity. While the exposure times
719 were typically set to these specified values, slight variations were occasionally made to optimize
720 imaging based on the levels of fluorescence expression observed.
721

722 For overexpression analysis, overnight cultures were diluted 1:500 into supplemented minimal
723 medium containing no added $MgSO_4$, 50 µg ml^{-1} carbenicillin, and either 500 µM IPTG or 0.5%
724 arabinose, as indicated. Cells were grown to the lag phase (OD_{600} ~0.005), then rapidly cooled
725 in an ice slurry before phase contrast microscopy. For empty vector control and start codon
726 variants, we captured lag phase micrograph images approximately 30-40 minutes post-
727 inoculation and -induction. For MgtS, MgrB, PmrR, YoaI, and YmiA overexpression, lag phase
728 measurements were performed at 2-3 hours, and for YkgS and DinQ, at 1-hour post-inoculation
729 and -induction. To concentrate the cells, 1 mL of the culture was pelleted and resuspended in
730 30-50 µL minimal A salt solution. For exponential phase analysis (OD_{600} between 0.2-0.4) in
731 cultures carrying empty vector control and start codon variants images were taken at ~3-4
732 hours. In the case of cells expressing MgtS, MgrB, PmrR, YoaI, and YmiA, images were taken
733 at 16-18 hours, and YkgS and DinQ at 6-8 hours. Microscope slides were prepared using 1%
734 agarose pads as described previously (Yadavalli *et al*, 2016), with approximately 5-7 µL of the
735 resuspended cells. A 40 ms exposure time and 20% intensity were applied to capture the
736 phase-contrast images.
737
738 For single-cell fluorescence measurements of wild type and Δ*yoaI* cells carrying P_{omrB}-*mScarlet*
739 reporter, overnight cultures were diluted 1:500 into fresh supplemented minimal A medium
740 containing either 10 mM or no added $MgSO_4$. Cells were grown to exponential (OD_{600} ~0.3 for
741 both stress and no stress conditions) and stationary phase (OD_{600} ~1.0 for stress condition and
742 ~3.5 for no stress condition), and then rapidly cooled in an ice slurry. Streptomycin was added
743 to a final concentration of 250 µg ml^{-1}. Fluorescence was measured using the mCherry channel
744 with an excitation wavelength of 570 nm and an emission filter of 645 nm. The exposure time
745 was set to 100 ms, with an intensity of 20%. Background fluorescence was determined by
746 imaging MG1655 cells grown under the same conditions.
747
748 For single-cell fluorescence measurements upon YoaI overexpression (to measure reporter
749 activities of P_{ompF}-*yfp* and P_{ompC}-*cfp*), the overnight cultures were diluted 1:500 into fresh
750 supplemented minimal A medium containing 10 mM $MgSO_4$. Cells were grown to exponential
751 phase (OD_{600} between 0.2-0.4), then rapidly cooled in an ice slurry, and streptomycin was added
752 at 250 µg ml^{-1}. YFP fluorescence was measured using a 500 nm excitation wavelength and a
753 535 nm emission filter. CFP fluorescence was measured using a 435 nm excitation wavelength
754 and a 480 nm emission filter. The exposure time for YFP and CFP measurements was set to 50
755 ms, respectively, with an intensity of 20%. The background fluorescence was determined by
756 imaging MG1655/pEB52 cells grown under the same conditions.
757
758 Image visualization and acquisition were performed using a Nikon Ti-E epifluorescence
759 microscope equipped with a TI2-S-HU attachable mechanical stage. The images were captured
760 with a Prime 95B sCMOS camera from Teledyne Photometrics with 1x1 binning. All image
761 acquisition was managed using Metamorph software (Molecular Devices), version 7.10.3.279. A
762 minimum of 50 cells per replicate were analyzed for cell volume and single-cell fluorescence
763 quantification. The distributions of cellular volume were assumed to follow the sphero-cylindrical
764 shape of *E. coli.* The volume was calculated using the formula $\mathrm{V} = \frac{\mathrm{pi}}{4} * \mathrm{W}^2 * \left(\mathrm{L} - \frac{\mathrm{W}}{3}\right)$. Images

765 were analyzed, and the cellular length, width, and fluorescence intensity were quantified using
766 ImageJ (Schneider *et al*, 2012) and MicrobeJ plugin (Jiang *et al*, 2014).
767
768 **Preparation of membrane and cytoplasmic fractions**
769 Membrane and cytoplasmic protein fractions were prepared as described previously (Yadavalli
770 Srujana S. *et al*, 2020). Briefly, saturated cultures of MG1655/pSV14 (PmrR-GGSG-6XHis),
771 MG1655/pSV26 (YobF-GGSG-6XHis), and MG1655/pEB52 (empty vector) were diluted 1:500
772 in 4 ml of LB media containing 100 µg ml^{-1} carbenicillin and grown at 37 °C. After 4 hours of
773 growth, 0.5 mM IPTG was added to the cultures, and the cells were harvested after 2 hours of
774 induction. Cell pellets were resuspended in 50 µl of cold resuspension buffer containing 20%
775 sucrose, 30 mM Tris pH 8.0, and 1X protease inhibitor cocktail (Sigma, cOmplete, EDTA-free).
776 Then, 50 µl of 10 mg ml^{-1} lysozyme, freshly prepared in 0.1 M EDTA pH 7.0, was added to the
777 cell suspension, and the mixture was incubated on ice for 30 minutes. Next, 1 ml of 3 mM EDTA
778 pH 7.5 was added to each sample, followed by sonication (10s pulse, 10s gap, 6 times) using
779 VCX-130 Vibra-Cell Ultrasonic sonicator (Fisher Scientific). Samples were briefly centrifuged at
780 6,000 rpm for 10 minutes at 4 °C to remove cellular debris, and the supernatant was collected
781 and spun at 21,000 ×g for 30 minutes at 4 °C. The supernatant from this step is separated and
782 stored as the cytoplasmic fraction. The pellet, representing the membrane fraction, was
783 resuspended in a storage buffer containing 20 mM Tris pH 8.0/20% glycerol. For strains
784 carrying genomic YoaI-SPA translational fusion, cultures were grown to an OD_{600} of ~0.2-0.4
785 before harvesting, and membrane and cytoplasmic fractions were prepared as mentioned
786 above.
787
788 **Western blot analysis**
789 The membrane and cytoplasmic fractions were resuspended in 4X Laemmli sample buffer
790 containing 5% 2-mercaptoethanol and no dyes. The samples were heated at 70 °C for 10
791 minutes and run on a 12% Bis-Tris gel (NuPage, Invitrogen) using MES running buffer
792 (Invitrogen) at 160V for 80 minutes. After electrophoresis, proteins were transferred to a PVDF
793 membrane (Amersham™ Hybond™) with a 0.2 µm pore size using a semi-dry transfer cell (Bio-
794 Rad Trans-Blot SD). The membranes were blocked with 5% w/v milk in Tris-buffered saline, pH
795 7.4, with 1% Tween 20 (TBS-T). Primary antibodies – mouse M2 anti-FLAG (Sigma-Aldrich) and
796 rabbit anti-6XHis tag antibody (Rockland) were used at 1:1000 dilution to detect SPA- and
797 6XHis-tagged constructs, respectively. IRDye 800CW goat anti-mouse and IRDye 680RD
798 donkey anti-rabbit antibodies (LiCOR) were used for secondary detection. SeaBlue™ Plus2 Pre-
799 stained Protein Standard (Invitrogen) was used as a ladder to visualize lower molecular weight
800 protein bands. The proteins were visualized using a LI-COR Odyssey imager.
801
802 **Bacterial two-hybrid and β-galactosidase reporter gene assays**
803 For the bacterial two-hybrid assay, several clones from the transformation plate were picked to
804 reduce heterogeneity (Battesti & Bouveret, 2012) and inoculated in LB containing 100 µg ml^{-1}
805 ampicillin and 50 µg ml^{-1} kanamycin. Cultures were grown overnight at 30°C with shaking. The
806 cultures were then diluted 1:1000 into LB supplemented with 500 µM IPTG and grown at 30°C
807 until OD_{600} reached between 0.2-0.4, after which β-galactosidase activities (Miller units) were
808 measured as previously described (Thibodeau *et al*, 2004).

For the β-galactosidase reporter gene assay, strains carrying P_{omrB}-*lacZ* with either pSV34 (pYoaI) or pEB52 (empty vector) were grown overnight in LB medium with 100 µg ml^{-1} ampicillin. The next day, the cultures were diluted 1:100 in the same medium and grown at 37 °C. After 3 hours of growth, 0.5 mM IPTG was added to the cultures, and the cells were harvested after 2 hours of induction. For high-throughput measurements in a 96-well format, the protocol was modified as previously described (Thibodeau *et al*, 2004).

Resource availability

Lead contact

Further information and requests for resources and reagents should be directed to and will be fulfilled by the lead contact, Srujana S. Yadavalli (sam.yadavalli@rutgers.edu).

Materials availability

Requests for strains and plasmids generated in this study should be directed to and will be fulfilled by the lead contact, Srujana S. Yadavalli (sam.yadavalli@rutgers.edu).

Data and code availability

Next-generation sequencing data generated in this study are deposited at Gene Expression Omnibus (GEO) with accession number GSE276379. All data generated or analyzed during this study are included in the manuscript and its supporting files. Source data files for all figures have been provided. The code used for data processing and analysis is available in a series of R Markdown documents hosted on GitHub (https://github.com/yadavalli-lab/Small-proteins-induced-under-low-magnesium-stress-in-E.coli).

Acknowledgments

The authors would like to thank Drs. Mark Goulian, Bryce Nickels, Gisela Storz, and Maude Guillier for generously sharing strains and plasmids. We thank Dr. Goulian, and the past and present members of the Yadavalli, Storz, and Shah Labs for their input and helpful discussions. Funding: S.S.Y. is supported by the National Institutes of Health - National Institute of General Medical Sciences (NIH-NIGMS) ESI-MIRA R35 GM147566 and institutional start-up funds from Rutgers. P.S. was supported by NIH/NIGMS grant R35 GM124976 and start-up funds from the Human Genetics Institute of New Jersey at Rutgers University. S.V. is supported by the Waksman Institute Busch Predoctoral fellowship (2022-24). The funders did not play any role in the study design, data collection and analysis, decision to publish, or preparation of the manuscript.

Author contributions

S.V., P.S., and S.S.Y. conceived the experiments. All authors planned the experiments, designed the methodology, and performed data analysis. S.V., P.S., and S.S.Y. wrote the initial draft of the manuscript, P.S. contributed to revisions and editing, and all authors reviewed the final manuscript.

Disclosure and competing interests statement

The authors declare no competing interests. P.S. is a director at an RNA-therapeutics startup.

References

Alphen WV & Lugtenberg B (1977) Influence of osmolarity of the growth medium on the outer membrane protein pattern of Escherichia coli. *J Bacteriol* 131: 623–630

Banerjee T (2022) Regulation of Gene Expression in Prokaryotes. In *Genetics Fundamentals Notes* pp 569–596. Singapore: Springer Nature Singapore

Bastet L, Korepanov AP, Jagodnik J, Grondin JP, Lamontagne A-M, Guillier M & Lafontaine DA (2024) Riboswitch and small RNAs modulate btuB translation initiation in Escherichia coli and trigger distinct mRNA regulatory mechanisms. *Nucleic Acids Res* 52: 5852–5865

Batchelor E, Silhavy TJ & Goulian M (2004) Continuous control in bacterial regulatory circuits. *J Bacteriol* 186: 7618–7625

Batchelor E, Walthers D, Kenney LJ & Goulian M (2005) The Escherichia coli CpxA-CpxR envelope stress response system regulates expression of the porins ompF and ompC. *J Bacteriol* 187: 5723–5731

Battesti A & Bouveret E (2012) The bacterial two-hybrid system based on adenylate cyclase reconstitution in Escherichia coli. *Methods* 58: 325–334

Baumberg S ed. (1999) Prokaryotic Gene Expression. doi:10.1093/oso/9780199636044.001.0001 [PREPRINT]

Bray NL, Pimentel H, Melsted P & Pachter L (2016) Near-optimal probabilistic RNA-seq quantification. *Nat Biotechnol* 34: 525–527

Burton AT, Zeinert R & Storz G (2024) Large Roles of Small Proteins. *Annu Rev Microbiol*

Cain JA, Solis N & Cordwell SJ (2014) Beyond gene expression: the impact of protein post-translational modifications in bacteria. *J Proteomics* 97: 265–286

Cannatelli A, Giani T, D'Andrea MM, Di Pilato V, Arena F, Conte V, Tryfinopoulou K, Vatopoulos A, Rossolini GM & COLGRIT Study Group (2014) MgrB inactivation is a common mechanism of colistin resistance in KPC-producing Klebsiella pneumoniae of clinical origin. *Antimicrob Agents Chemother* 58: 5696–5703

Carlberg C & Molnar F (2016) Mechanisms of Gene Regulation 2nd ed. Dordrecht, Netherlands: Springer

Chekabab SM, Jubelin G, Dozois CM & Harel J (2014) PhoB activates Escherichia coli O157:H7 virulence factors in response to inorganic phosphate limitation. *PLoS One* 9: e94285

893 Chen AI, Albicoro FJ, Zhu J & Goulian M (2021) Effects of regulatory network organization and
894 environment on PmrD connector activity and polymyxin resistance in Klebsiella
895 pneumoniae and Escherichia coli. *Antimicrob Agents Chemother* 65

896 Cherepanov PP & Wackernagel W (1995) Gene disruption in Escherichia coli: TcR and KmR
897 cassettes with the option of Flp-catalyzed excision of the antibiotic-resistance
898 determinant. *Gene* 158: 9–14

899 Cope AL, Vellappan S, Favate JS, Skalenko KS, Yadavalli SS & Shah P (2022) Exploring
900 Ribosome-Positioning on Translating Transcripts with Ribosome Profiling. *Methods Mol*
901 *Biol* 2404: 83–110

902 Datsenko KA & Wanner BL (2000) One-step inactivation of chromosomal genes in Escherichia
903 coli K-12 using PCR products. *Proc Natl Acad Sci U S A* 97: 6640–6645

904 Eguchi Y, Itou J, Yamane M, Demizu R, Yamato F, Okada A, Mori H, Kato A & Utsumi R (2007)
905 B1500, a small membrane protein, connects the two-component systems EvgS/EvgA
906 and PhoQ/PhoP in *Escherichia coli*. *Proc Natl Acad Sci U S A* 104: 18712–18717

907 Feilmeier BJ, Iseminger G, Schroeder D, Webber H & Phillips GJ (2000) Green fluorescent
908 protein functions as a reporter for protein localization in Escherichia coli. *J Bacteriol* 182:
909 4068–4076

910 Fitzgerald DM, Stringer AM, Smith C, Lapierre P & Wade JT (2023) Genome-Wide Mapping of
911 the Escherichia coli PhoB Regulon Reveals Many Transcriptionally Inert, Intragenic
912 Binding Sites. *MBio* 14: e0253522

913 Gardner SG & McCleary WR (2019) Control of the phoBR Regulon in Escherichia coli. *EcoSal*
914 *Plus* 8

915 Gerken H, Charlson ES, Cicirelli EM, Kenney LJ & Misra R (2009) MzrA: a novel modulator of
916 the EnvZ/OmpR two-component regulon. *Mol Microbiol* 72: 1408–1422

917 Glaub A, Huptas C, Neuhaus K & Ardern Z (2020) Recommendations for bacterial ribosome
918 profiling experiments based on bioinformatic evaluation of published data. *J Biol Chem*
919 295: 8999–9011

920 Godiska R, Patterson M, Schoenfeld T, and Mead DA (2005) Beyond pUC: Vectors for Cloning
921 Unstable DNA. In *DNA Sequencing: Optimizing the Process and Analysis*, Kieleczawa J
922 (ed) pp 55–76. Sudbury, Massachusetts: Jones & Bartlett Learning

923 Gottesman S (2019) Trouble is coming: Signaling pathways that regulate general stress
924 responses in bacteria. *J Biol Chem* 294: 11685–11700

925 Goulian M (2010) Two-component signaling circuit structure and properties. *Curr Opin Microbiol*
926 13: 184–189

927 Gray T, Storz G & Papenfort K (2022) Small Proteins; Big Questions. *J Bacteriol* 204: e0034121

928 Groisman EA (2001) The pleiotropic two-component regulatory system PhoP-PhoQ. *J Bacteriol*
929 183: 1835–1842

930 Groisman EA & Chan C (2021) Cellular Adaptations to Cytoplasmic Mg2+ Limitation. *Annu Rev*
931 *Microbiol* 75: 649–672

932 Groisman EA, Duprey A & Choi J (2021) How the PhoP/PhoQ System Controls Virulence and
933 Mg2+ Homeostasis: Lessons in Signal Transduction, Pathogenesis, Physiology, and
934 Evolution. *Microbiol Mol Biol Rev* 85: e0017620

935 Hemm Matthew R., Weaver Jeremy, Storz Gisela, Lovett Susan T. & Hinton Deborah (2020)
936 Escherichia coli Small Proteome. *EcoSal Plus* 9

937 Hemm MR, Paul BJ, Miranda-Ríos J, Zhang A, Soltanzad N & Storz G (2010) Small stress
938 response proteins in Escherichia coli: proteins missed by classical proteomic studies. *J*
939 *Bacteriol* 192: 46–58

940 Hemm MR, Paul BJ, Schneider TD, Storz G & Rudd KE (2008) Small membrane proteins found
941 by comparative genomics and ribosome binding site models. *Mol Microbiol* 70: 1487–
942 1501

943 Hobbs EC, Astarita JL & Storz G (2010) Small RNAs and small proteins involved in resistance
944 to cell envelope stress and acid shock in Escherichia coli: analysis of a bar-coded
945 mutant collection. *J Bacteriol* 192: 59–67

946 Hong X, Chen HD & Groisman EA (2018) Gene expression kinetics governs stimulus-specific
947 decoration of the *Salmonella* outer membrane. *Sci Signal* 11

948 Ikeda M, Arai M, Okuno T & Shimizu T (2003) TMPDB: a database of experimentally-
949 characterized transmembrane topologies. *Nucleic Acids Res* 31: 406–409

950 Jiang C, Brown PJB, Ducret A & Brun YV (2014) Sequential evolution of bacterial morphology
951 by co-option of a developmental regulator. *Nature* 506: 489–493

952 Käll L, Krogh A & Sonnhammer ELL (2004) A combined transmembrane topology and signal
953 peptide prediction method. *J Mol Biol* 338: 1027–1036

954 Karimova G, Pidoux J, Ullmann A & Ladant D (1998) A bacterial two-hybrid system based on a
955 reconstituted signal transduction pathway. *Proc Natl Acad Sci U S A* 95: 5752–5756

956 Kastenmayer JP, Ni L, Chu A, Kitchen LE, Au W-C, Yang H, Carter CD, Wheeler D, Davis RW,
957 Boeke JD, *et al* (2006) Functional genomics of genes with small open reading frames
958 (sORFs) in S. cerevisiae. *Genome Res* 16: 365–373

959 Kato A, Chen HD, Latifi T & Groisman EA (2012) Reciprocal control between a bacterium's
960 regulatory system and the modification status of its lipopolysaccharide. *Mol Cell* 47:
961 897–908

962 Kato A & Groisman EA (2004) Connecting two-component regulatory systems by a protein that
963 protects a response regulator from dephosphorylation by its cognate sensor. *Genes Dev*
964 18: 2302–2313

965 Kato A, Tanabe H & Utsumi R (1999) Molecular characterization of the PhoP-PhoQ two-
966 component system in Escherichia coli K-12: identification of extracellular Mg2+-
967 responsive promoters. *J Bacteriol* 181: 5516–5520

968 Kenney LJ & Anand GS (2020) EnvZ/OmpR Two-Component Signaling: An Archetype System
969 That Can Function Noncanonically. *EcoSal Plus* 9

970 Kim D, Paggi JM, Park C, Bennett C & Salzberg SL (2019) Graph-based genome alignment and
971 genotyping with HISAT2 and HISAT-genotype. *Nat Biotechnol* 37: 907–915

972 Kox LF, Wösten MM & Groisman EA (2000) A small protein that mediates the activation of a
973 two-component system by another two-component system. *EMBO J* 19: 1861–1872

974 Laub MT (2014) The role of two-component signal transduction systems in bacterial stress
975 responses. In *Bacterial Stress Responses* pp 45–58. Washington, DC, USA: ASM Press

976 Lippa AM & Goulian M (2009) Feedback inhibition in the PhoQ/PhoP signaling system by a
977 membrane peptide. *PLoS Genet* 5: e1000788

978 Love MI, Huber W & Anders S (2014) Moderated estimation of fold change and dispersion for
979 RNA-seq data with DESeq2. *Genome Biol* 15: 550

980 Martin M (2011) Cutadapt removes adapter sequences from high-throughput sequencing reads.
981 *EMBnet.journal* 17: 10–12

982 Meydan S, Marks J, Klepacki D, Sharma V, Baranov PV, Firth AE, Margus T, Kefi A, Vázquez-
983 Laslop N & Mankin AS (2019) Retapamulin-Assisted Ribosome Profiling Reveals the
984 Alternative Bacterial Proteome. *Mol Cell* 74: 481-493.e6

985 Miller JH & Others (1992) A Short Course in Bacterial Genetics: A Laboratory Manual and
986 Handbook for Escherichia Coli and Related Bacteria CSHL Press

987 Möller S, Croning MD & Apweiler R (2001) Evaluation of methods for the prediction of
988 membrane spanning regions. *Bioinformatics* 17: 646–653

989 Ochman H, Medhora MM, Garza D & Hartl DL (1990) Amplification of flanking sequences by
990 inverse PCR. *PCR protocols: A guide to methods and applications*: 219–227

991 Olaitan AO, Morand S & Rolain J-M (2014) Mechanisms of polymyxin resistance: acquired and
992 intrinsic resistance in bacteria. *Front Microbiol* 5: 643

993 Patel V & Matange N (2021) Adaptation and compensation in a bacterial gene regulatory
994 network evolving under antibiotic selection. *Elife* 10

995 Patraquim P, Mumtaz MAS, Pueyo JI, Aspden JL & Couso J-P (2020) Developmental regulation
996 of canonical and small ORF translation from mRNAs. *Genome Biol* 21: 128

997 Pontes MH & Groisman EA (2018) Protein synthesis controls phosphate homeostasis. *Genes*
998 *Dev* 32: 79–92

999 Pueyo JI, Magny EG & Couso JP (2016) New peptides under the s(ORF)ace of the genome.
1000 *Trends Biochem Sci* 41: 665–678

1001 Rubin EJ, Herrera CM, Crofts AA & Trent MS (2015) PmrD is required for modifications to
1002 escherichia coli endotoxin that promote antimicrobial resistance. *Antimicrob Agents*
1003 *Chemother* 59: 2051–2061

1004 Sberro H, Fremin BJ, Zlitni S, Edfors F, Greenfield N, Snyder MP, Pavlopoulos GA, Kyrpides
1005 NC & Bhatt AS (2019) Large-Scale Analyses of Human Microbiomes Reveal Thousands
1006 of Small, Novel Genes. *Cell* 178: 1245-1259.e14

1007 Schneider CA, Rasband WS & Eliceiri KW (2012) NIH Image to ImageJ: 25 years of image
1008 analysis. *Nat Methods* 9: 671–675

1009 Seshasayee ASN, Sivaraman K & Luscombe NM (2011) An overview of prokaryotic
1010 transcription factors : a summary of function and occurrence in bacterial genomes.
1011 *Subcell Biochem* 52: 7–23

1012 Smith T, Heger A & Sudbery I (2017) UMI-tools: modeling sequencing errors in Unique
1013 Molecular Identifiers to improve quantification accuracy. *Genome Res* 27: 491–499

1014 Steinberg R & Koch H-G (2021) The largely unexplored biology of small proteins in pro- and
1015 eukaryotes. *FEBS J* 288: 7002–7024

1016 Stock AM, Robinson VL & Goudreau PN (2000) Two-component signal transduction. *Annu Rev*
1017 *Biochem* 69: 183–215

1018 Storz G, Vogel J & Wassarman KM (2011) Regulation by small RNAs in bacteria: expanding
1019 frontiers. *Mol Cell* 43: 880–891

1020 Thibodeau SA, Fang R & Joung JK (2004) High-throughput beta-galactosidase assay for
1021 bacterial cell-based reporter systems. *Biotechniques* 36: 410–415

1022 Tian X, Manat G, Gasiorowski E, Auger R, Hicham S, Mengin-Lecreulx D, Boneca IG & Touzé T
1023 (2021) LpxT-Dependent Phosphorylation of Lipid A in Escherichia coli Increases
1024 Resistance to Deoxycholate and Enhances Gut Colonization. *Front Microbiol* 12: 676596

1025 Tollerson R 2nd & Ibba M (2020) Translational regulation of environmental adaptation in
1026 bacteria. *J Biol Chem* 295: 10434–10445

1027 Wang H, Yin X, Wu Orr M, Dambach M, Curtis R & Storz G (2017) Increasing intracellular
1028 magnesium levels with the 31-amino acid MgtS protein. *Proc Natl Acad Sci U S A* 114:
1029 5689–5694

1030 Weaver J, Mohammad F, Buskirk AR & Storz G (2019) Identifying Small Proteins by Ribosome
1031 Profiling with Stalled Initiation Complexes. *MBio* 10

1032 Weel-Sneve R, Kristiansen KI, Odsbu I, Dalhus B, Booth J, Rognes T, Skarstad K & Bjørås M
1033 (2013) Single transmembrane peptide DinQ modulates membrane-dependent activities.
1034 *PLoS Genet* 9: e1003260

1035 Yadavalli Srujana S., Goh Ted, Carey Jeffrey N., Malengo Gabriele, Vellappan Sangeevan,
1036 Nickels Bryce E., Sourjik Victor, Goulian Mark, Yuan Jing & Silhavy Thomas J. (2020)
1037 Functional Determinants of a Small Protein Controlling a Broadly Conserved Bacterial
1038 Sensor Kinase. *J Bacteriol* 202: e00305-20

1039 Yadavalli SS, Carey JN, Leibman RS, Chen AI, Stern AM, Roggiani M, Lippa AM & Goulian M
1040 (2016) Antimicrobial peptides trigger a division block in Escherichia coli through
1041 stimulation of a signalling system. *Nat Commun* 7: 1–10

1042 Yadavalli SS & Yuan J (2022) Bacterial Small Membrane Proteins: the Swiss Army Knife of
1043 Regulators at the Lipid Bilayer. *J Bacteriol* 204: e0034421

1044 Yin X, Wu Orr M, Wang H, Hobbs EC, Shabalina SA & Storz G (2019) The small protein MgtS
1045 and small RNA MgrR modulate the PitA phosphate symporter to boost intracellular
1046 magnesium levels. *Mol Microbiol* 111: 131–144

1047 Yoshida Y, Sugiyama S, Oyamada T, Yokoyama K & Makino K (2012) Novel members of the
1048 phosphate regulon in Escherichia coli O157:H7 identified using a whole-genome
1049 shotgun approach. *Gene* 502: 27–35

1050 Zhu A, Ibrahim JG & Love MI (2019) Heavy-tailed prior distributions for sequence count data:
1051 removing the noise and preserving large differences. *Bioinformatics* 35: 2084–2092

1052
1053
1054
1055
1056
1057
1058
1059
1060
1061
1062
1063
1064
1065
1066
1067
1068
1069
1070
1071
1072
1073
1074
1075
1076
1077
1078
1079
1080
1081
1082
1083
1084
1085
1086

1087 Figures and tables

1088

1089

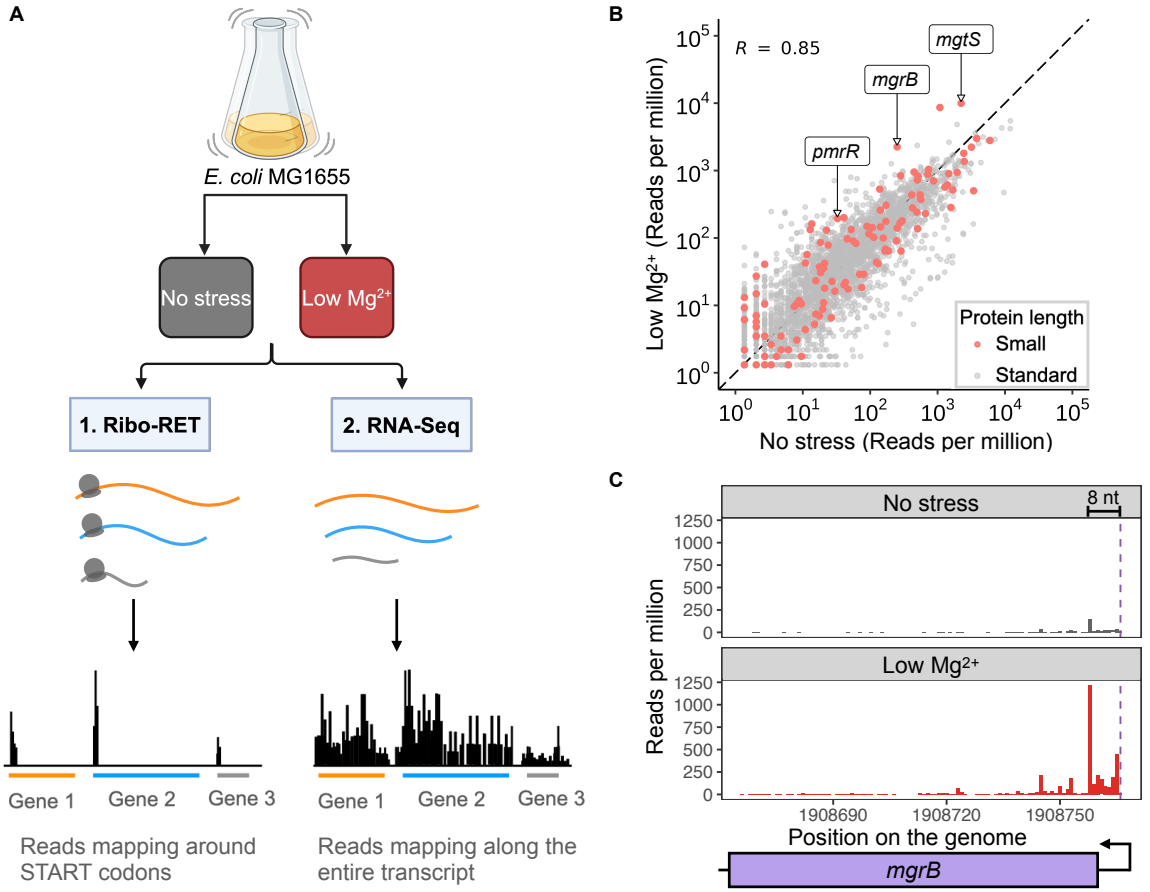

1090

1091

1092 **Figure 1. Identification of small proteins induced under low magnesium stress in *E. coli***
1093 **by translation-initiation profiling (Ribo-RET).** (A) Schematic diagram showing the Ribo-RET
1094 and RNA-Seq experimental setup used to identify small proteins induced by low magnesium
1095 stress. Wild-type *E. coli* K-12 MG1655 cells were grown in supplemented minimal A medium
1096 containing $MgSO_4$ at either 10 mM (no stress) or ~1 μM (no added magnesium, low Mg^{2+}
1097 stress). (B) Scatterplot showing the correlation between the Ribo-RET reads mapping to the
1098 annotated start sites of proteins expressed under low Mg^{2+} stress and no stress. The red dots
1099 represent annotated small proteins of ≤ 50 amino acids in length, and the gray dots represent
1100 proteins > 50 amino acids long. Small proteins, MgrB, MgtS, and PmrR, known to be induced
1101 under magnesium starvation, are highlighted. Pearson's coefficient, r= 0.85. (C) Ribo-RET data
1102 for a representative small protein MgrB induced under low Mg^{2+} stress. A purple dashed line
1103 indicates the translation start site, and the 8 nucleotide (nt) indicates the distance between the
1104 highest ribosome density peak and the first nucleotide of the start codon. (Also see Tables 1,
1105 S4, Fig. S1 and S2)

1106

1107

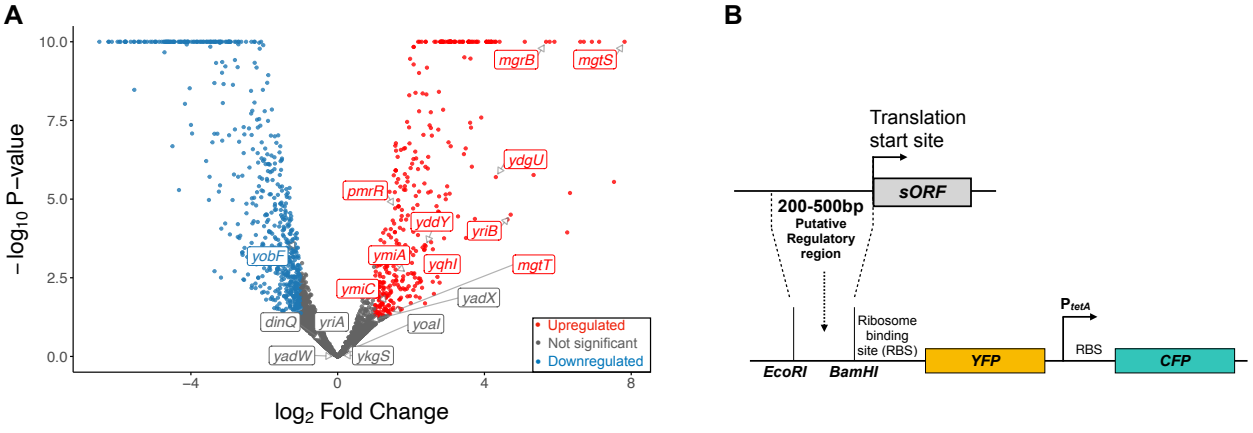
A
B
10.0
7.5
5.0
2.5
0.0
−4
0
4
8
− log10 P−value
log2 Fold Change
mgrB
mgtS
ydgU
pmrR
yddY
yriB
ymiA
yghI
mgtT
ymiC
yadX
yobF
dinQ
yriA
yoaI
yadW
ykgS
Upregulated
Not significant
Downregulated
Translation
start site
sORF
200-500bp
Putative
Regulatory
region
Ribosome
binding
site (RBS)
PtetA
RBS
EcoRI
BamHI
YFP
CFP

1108

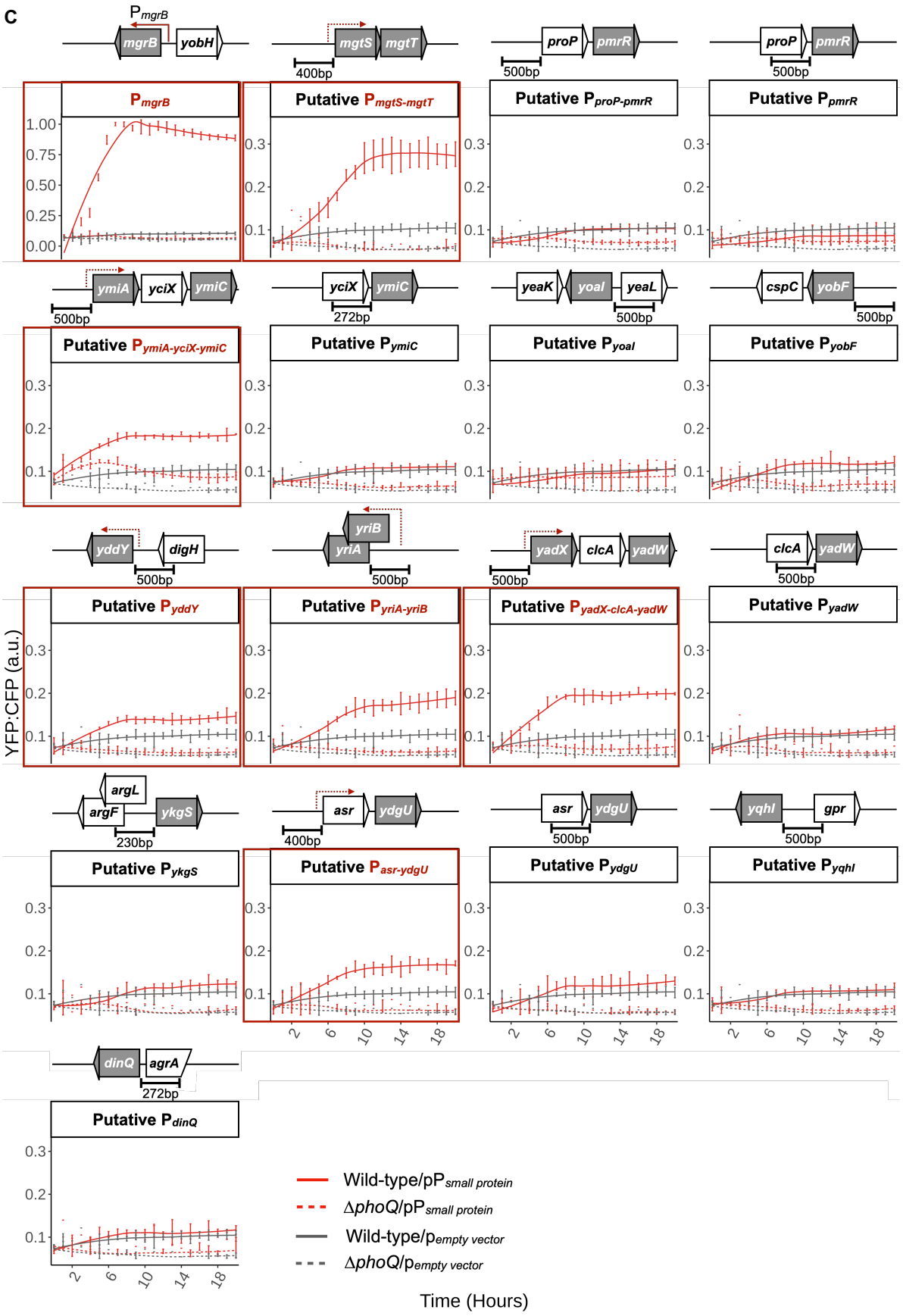
C
PmgrB
mgrB
yobH
mgtS
mgtT
400bp
proP
pmrR
500bp
PmgrB
Putative PmgtS-mgtT
Putative PproP-pmrR
Putative PpmrR
ymiA
yciX
ymiC
272bp
yeaK
yoaI
yeaL
cspC
yobF
Putative PymiA-yciX-ymiC
Putative PymiC
Putative PyoaI
Putative PyobF
yddY
digH
yriB
yriA
yadX
clcA
yadW
Putative PyddY
Putative PyriA-yriB
Putative PyadX-clcA-yadW
Putative PyadW
YFP:CFP (a.u.)
argL
argF
ykgS
230bp
asr
ydgU
yqhI
gpr
Putative PykgS
Putative Pasr-ydgU
Putative PydgU
Putative PyqhI
dinQ
agrA
Putative PdinQ
Wild-type/pPsmall protein
ΔphoQ/pPsmall protein
Wild-type/pempty vector
ΔphoQ/pempty vector
Time (Hours)

1109

1110
1111 **Figure 2. Transcriptional regulation of small proteins induced under low magnesium**
1112 **stress.** (A) RNA-Seq analysis of transcripts representing small proteins induced under low
1113 magnesium stress. Volcano plot illustrating differential expression of small proteins induced
1114 under low magnesium stress from RNA-Seq data. Transcripts either upregulated or
1115 downregulated are highlighted in red or blue, respectively, and those with no significant change
1116 are represented in gray. The criteria for significance include a fold change threshold of >2 and a
1117 p-value of <0.05. The $-\log_{10}$ P-value of *mgrB* and *mgtS* were 75 and 140 respectively. To
1118 prevent distortion from their exceptionally high values dominating the plot, the transformed p-
1119 values were capped at 10 to enhance visualization. Data represent differential expression
1120 analysis from two independent replicates. (B) Schematic representation of the transcriptional
1121 reporter fusion construct. Regions (200-500 bp) upstream of the small open reading frames of
1122 interest were amplified from the MG1655 genome and cloned into a YFP-encoding reporter
1123 plasmid (pMR120) resulting in plasmids pPJ14, pPJ16-pPJ20, pPJ23, pSV16-pSV21, pSV24,
1124 pSV28-pSV29 (See Table S6 for genomic coordinates of the regulatory regions tested here and
1125 Table S2 for plasmid details). (C) Measurement of transcriptional reporter activity (YFP:CFP) for
1126 the indicated small proteins under low Mg^{2+} (no added magnesium). The solid and dashed lines
1127 represent the wild-type *E. coli* MG1655 and Δ*phoQ* cells, respectively, harboring plasmids with
1128 either transcriptional fusion for a putative regulatory region of a small protein with *yfp* (red line)
1129 or *yfp* only (gray line). The schematic above each plot depicts the arrangement of the small
1130 protein-encoding genes (shown in gray), including the putative regulatory regions and operons
1131 where applicable. Transcriptional reporters showing an increased activity compared to the
1132 empty vector control (pMR120) are highlighted in red. The cultures were grown in a
1133 supplemented minimal medium with 6 μg ml^{-1} chloramphenicol. The data represent averages
1134 and standard errors of the means for four independent replicates. (Also see Tables S4, S6, and
1135 Fig. S3)
1136
1137
1138
1139
1140

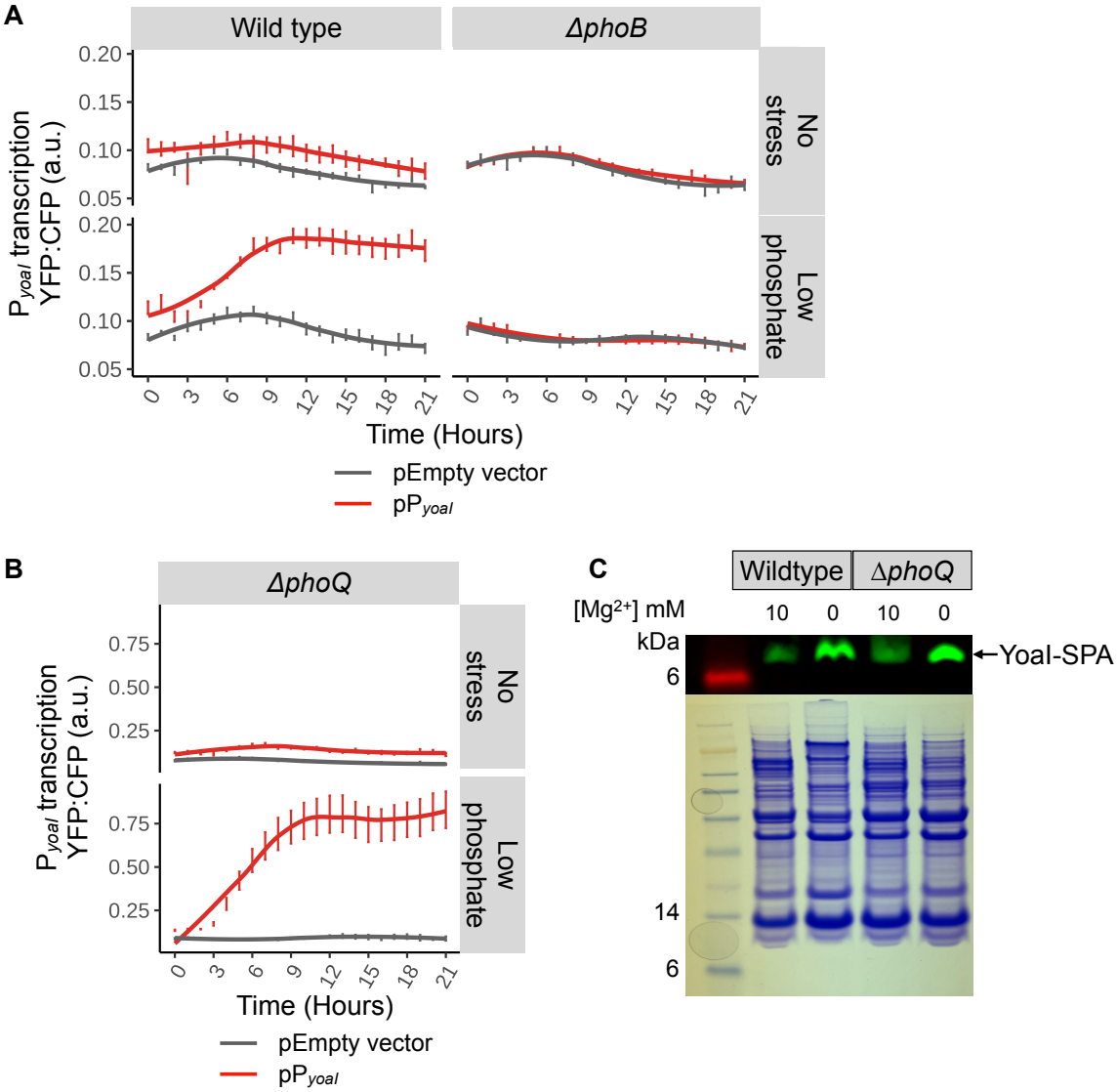

Figure 3. Regulation of YoaI expression during magnesium limitation. (A-B) Transcriptional activity of *yoaI* was measured as a function of YFP reporter fluorescence in *E. coli* MG1655, Δ*phoB* (SV48), and Δ*phoQ* (TIM100) strains under phosphate stress as indicated. The red and gray lines represent cells carrying plasmid-encoded P_{yoaI}-*yfp* transcriptional reporter (pPJ18) and *yfp*-only control vector (pMR120), respectively. The cultures were grown in a supplemented MOPS minimal medium with 6 μg ml^{-1} chloramphenicol with either 1 mM K_2HPO_4 for no stress condition, or no added K_2HPO_4 for phosphate stress. The data illustrate average YFP:CFP fluorescence with standard error of the means, derived from four independent replicates. (C) Detection of YoaI protein in *E. coli* wild-type (GSO317) and Δ*phoQ* (SV60) strains containing *yoaI-SPA* genomic translational fusion. Cells were grown in supplemented minimal A medium, with $MgSO_4$ added at the specified concentration (10mM or no added $MgSO_4$). Membrane fractions were analyzed by western blotting using M2 anti-FLAG antibodies (top) and by Coomassie Brilliant Blue staining (bottom). The data represent results from two independent replicates.

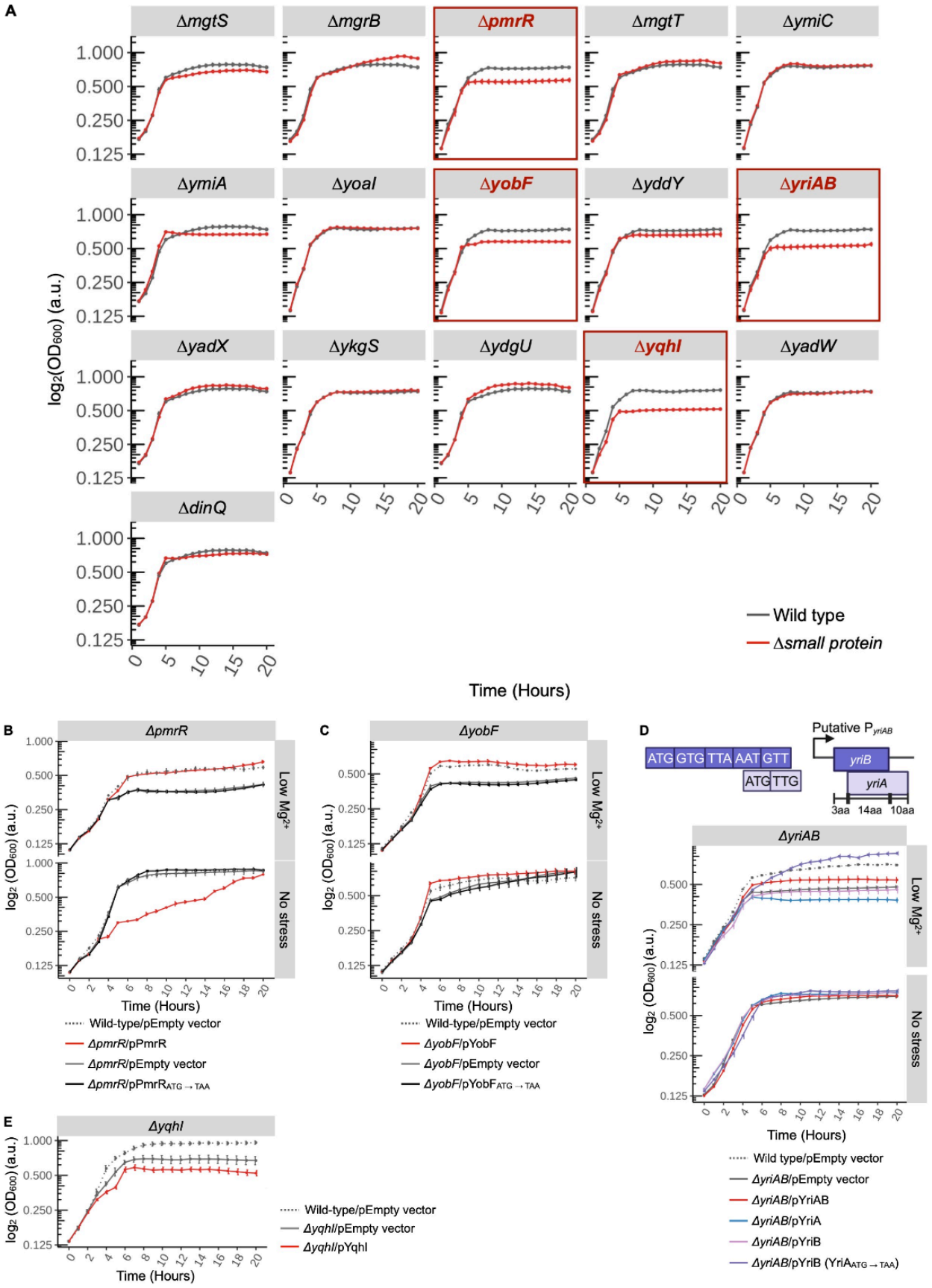
A
ΔmgtS
ΔmgrB
ΔpmrR
ΔmgtT
ΔymiC
ΔymiA
Δyoal
ΔyobF
ΔyddY
ΔyriAB
ΔyadX
ΔykgS
ΔydgU
Δyqhl
ΔyadW
ΔdinQ
log2(OD600) (a.u.)
Time (Hours)
Wild type
Δsmall protein
B
ΔpmrR
Low Mg2+
No stress
Wild-type/pEmpty vector
ΔpmrR/pPmrR
ΔpmrR/pEmpty vector
ΔpmrR/pPmrRATG → TAA
C
ΔyobF
ΔyobF/pYobF
ΔyobF/pEmpty vector
ΔyobF/pYobFATG → TAA
D
Putative PyriAB
ATG GTG TTA AAT GTT
ATG TTG
yriB
yriA
3aa 14aa 10aa
ΔyriAB
Wild type/pEmpty vector
ΔyriAB/pEmpty vector
ΔyriAB/pYriAB
ΔyriAB/pYriA
ΔyriAB/pYriB
ΔyriAB/pYriB (YriAATG → TAA)
E
Δyqhl
Wild-type/pEmpty vector
Δyqhl/pEmpty vector
Δyqhl/pYqhl

1157

1158
1159 **Figure 4. Effect of deleting genes encoding low Mg^{2+} stress-induced small proteins on**
1160 **bacterial growth.** (A) Growth curves of wild-type *E. coli* MG1655 (gray) and mutants
1161 corresponding to the deletions of small protein-encoding genes (red) (strains SV64, AML67,
1162 SV35, SV31, SV41, SV57, SV59, SV33, SV29, SV25, SV39, SV43, SV58, SV37, SV27, and
1163 SV56, please see Table S1 and methods for strain details). Deletion mutants showing reduced
1164 growth yield compared to wild-type cells are highlighted in red. The cultures were grown in
1165 supplemented minimal A medium with no added magnesium and 50 μg ml^{-1} carbenicillin. Data
1166 represent averages and standard errors of means for four independent cultures. (B-C)
1167 Complementation of growth phenotypes associated with *pmrR,* and *yobF* deletions. Growth
1168 curves of Δ*pmrR* (SV35), and Δ*yobF* (SV34) deletion strains carrying an empty vector (pEB52,
1169 solid gray line) or complemented with plasmids encoding small proteins pPmrR (pSV35) and
1170 pYobF (pJS5) (red line) or their variants $pPmrR_{ATG\rightarrow TAA}$ (pSV38), and $pYobF_{ATG\rightarrow TAA}$ (pSV45)
1171 (black line), as indicated. Wild-type MG1655 cells containing the empty vector are included as a
1172 control (dashed gray line). (D) Schematic of the overlapping genes *yriAB* followed by the growth
1173 curves of gene deletion *ΔyriAB* (SV25) complemented with pYriAB (pSV58), pYriA (pJS1), pYriB
1174 (pSV37), pYriB ($YriA_{ATG\rightarrow TAA}$) (pSV59), or an empty vector (pEB52, as indicated. (E) Growth
1175 curves of gene deletion *ΔyqhI* (SV37) carrying an empty vector (pEB52), or complemented with
1176 a plasmid encoding YqhI. Wild-type cells containing an empty vector (pEB52, dashed gray line)
1177 are included as a control. For panels A-D, cultures were grown in supplemented minimal A
1178 medium containing 50 μg ml^{-1} carbenicillin and either no added magnesium or 10 mM $MgSO_4$ as
1179 indicated. 500 μM IPTG was used for induction, except for PmrR derivatives (pSV35 and
1180 pSV38), where 12.5 μM IPTG was used. Data represent averages and standard errors of
1181 means for four independent cultures.
1182
1183

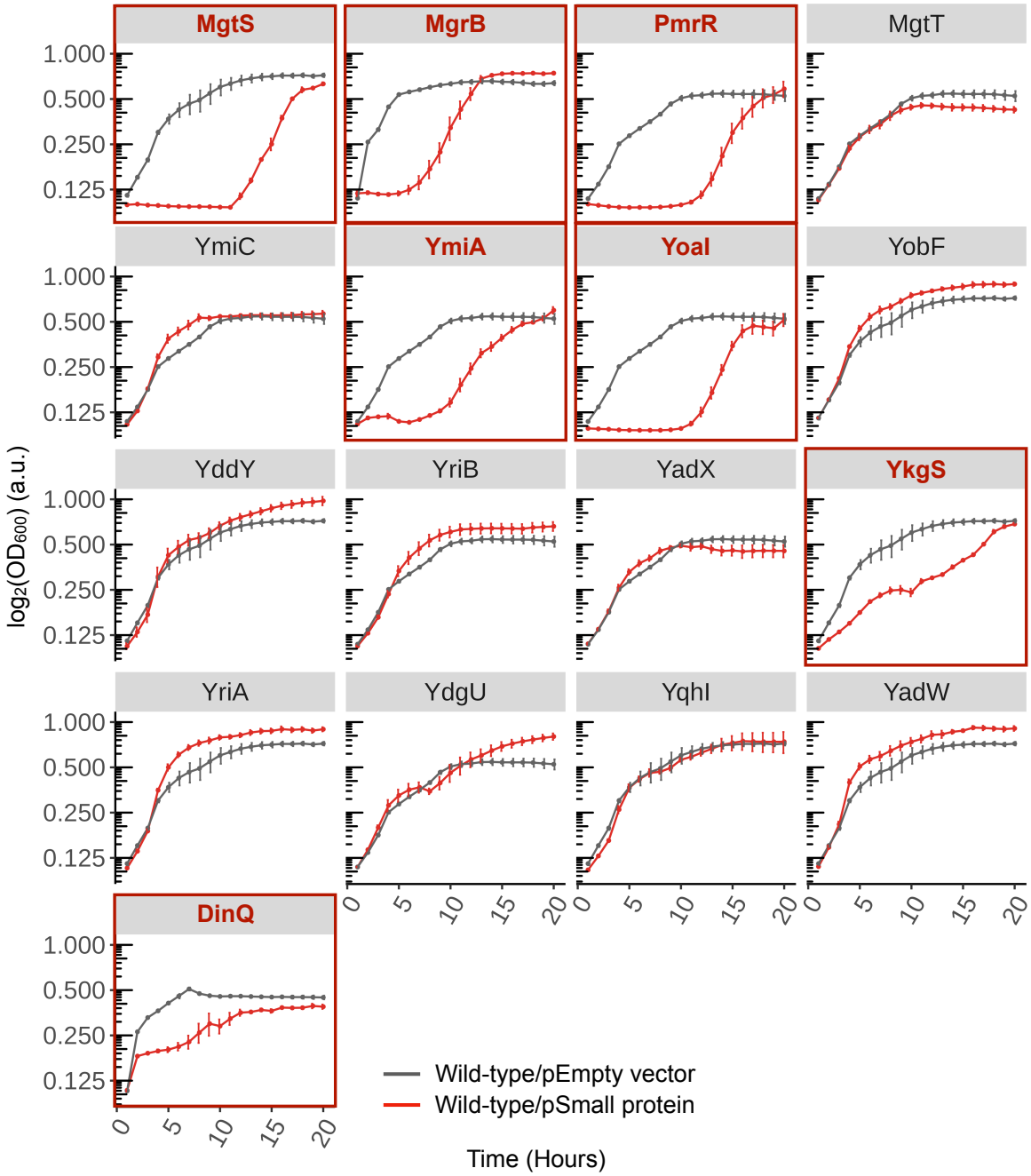

Figure 5. Effect of overexpression of low Mg^{2+} stress-induced small proteins on growth. Growth curves of *E. coli* MG1655 cells expressing each of the 17 stress-specific small proteins (encoded by plasmids pSV30-37, pSV54, pSV60, or pJS1-7; please see Table S2 for details) are represented in red, while cells carrying the empty vector (pEB52 and pBAD24) are shown in gray. The cells were grown under low Mg^{2+} stress (no added magnesium). Small proteins whose expression causes a growth defect or delay are highlighted in red. The cultures were grown in supplemented minimal A medium with 50 µg ml^{-1} carbenicillin. 500 µM IPTG was used as an inducer for all P_{trc}-based vectors, in the case of pSV54and pBAD24, 0.5% arabinose was used. Data represent averages and standard error of means for four independent cultures.

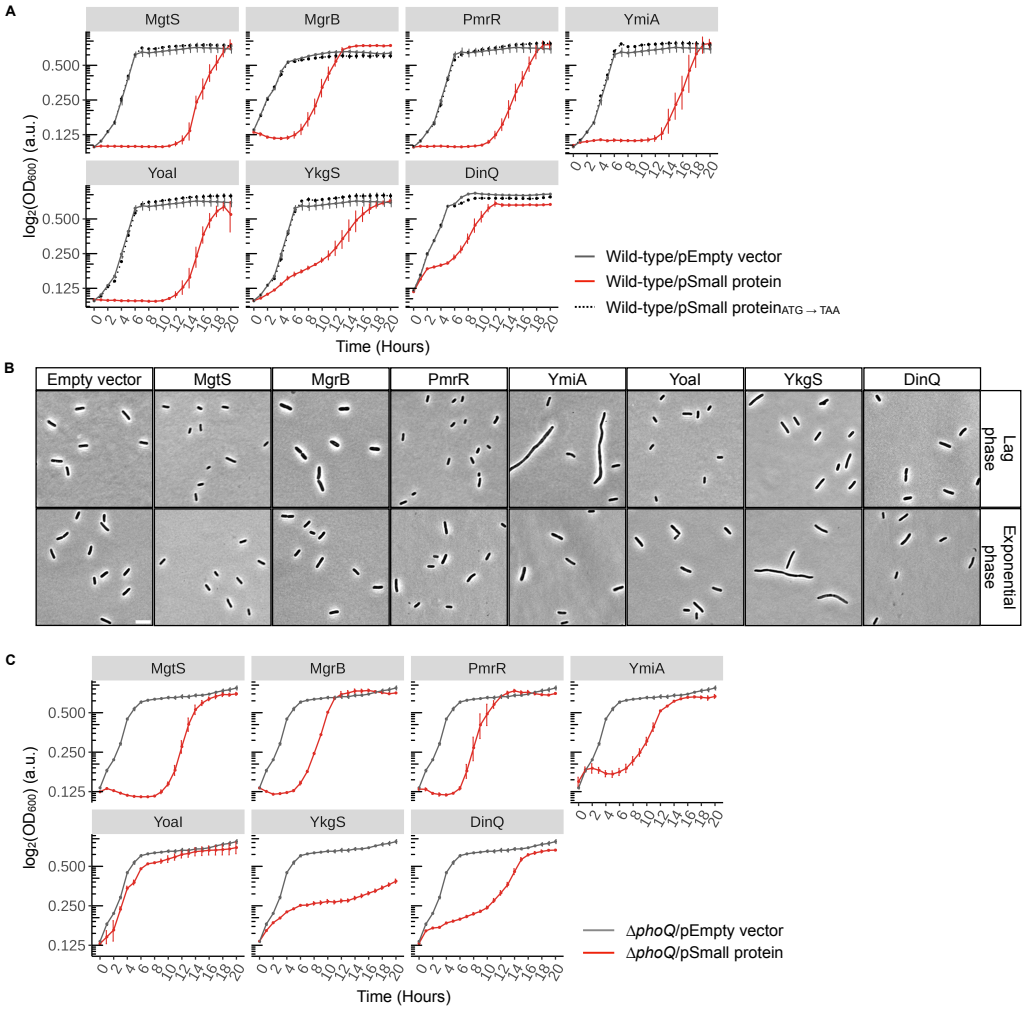

Figure 6. Analysis of growth defect and cell size changes associated with overexpression of small proteins, MgtS, MgrB, PmrR, YkgS, YoaI, YmiA and DinQ. (A) Growth curves of *E. coli* MG1655 cells expressing the indicated small proteins (red line) and empty vector control (pEB52 or pBAD24, gray line). The start codon (ATG) of each small protein is mutated to a stop codon (TAA), and the growth curves of cells expressing these constructs are depicted in dotted black. Plasmids pSV34-36, pSV38-42, pSV54-55, pSV60-61, or pJS4, pJS7 were used as applicable, please see Table S2 for details. Data represent averages and standard error of means for four independent cultures. (B) Representative phase contrast micrographs of the cells expressing small proteins during lag (top panel) and exponential phase (bottom panel) after induction, scale bar = 5 μm. Data is representative of three independent cultures. (C) Growth curves of Δ*phoQ* (TIM202) cells expressing the indicated small proteins (red line) and empty vector control (pEB52 or pBAD24, gray line). Plasmids pSV34-36, pSV54, pSV60, pJS4, and pJS7 were used as applicable, please see Table S2 for details. Data represent averages and standard error of means for four independent cultures. For panels A-C, the cultures were grown in supplemented minimal A medium containing no added magnesium, 50 μg ml^{-1} carbenicillin, and 500 μM IPTG for all P_{trc}-based vectors, except for pSV54 and pBAD24, where 0.5% arabinose was utilized instead. (Also see Fig. S6 and S7)

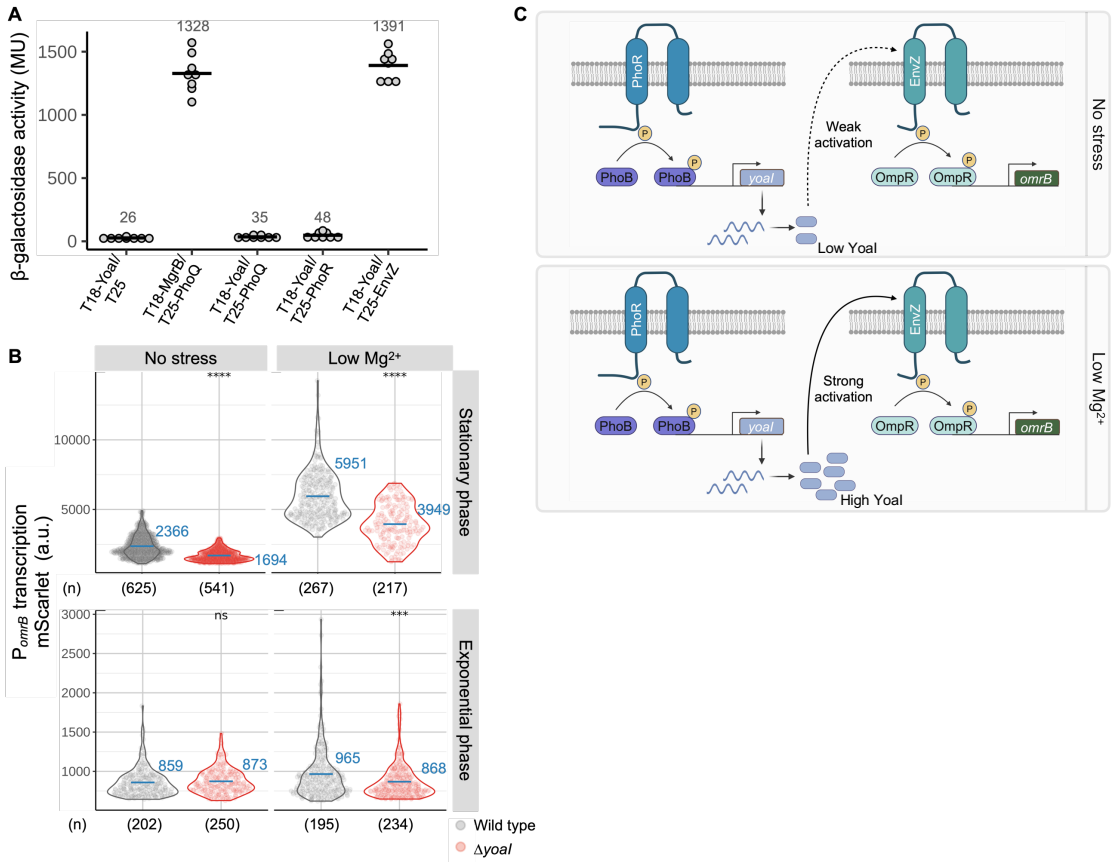

Figure 7. Effect of YoaI expression on the EnvZ-OmpR system. (A) BACTH assays were conducted using cells harboring T18 and T25 fusion proteins of *B. pertussis* adenylyl cyclase, in a *cyaA* mutant BACTH host strain, SAM85, which contains *lacI*^{q}. β-gal activity was measured to assess interactions between T18-YoaI (pSV47) and T25-linked PhoQ (pAL27), PhoR (pSY68), or EnvZ (pKK14). T25 alone was used as a negative control, and T18-MgrB (pAL33) combined with T25-PhoQ (pAL27) was used as a positive control. The cultures were grown in LB medium containing 50 μg ml^{-1} kanamycin, 100 μg ml^{-1} carbenicillin, and 500 μM IPTG. Each circle represents a biological replicate, with the mean values from two independent experiments indicated, expressed in Miller units (MU). (B) Transcriptional activity of *omrB* was measured as a function of mScarlet reporter fluorescence in *E. coli* MG1655 (SV97), and Δ*yoaI* (SV95) strains at the stationary phase (top panel) and exponential phase (bottom panel). Each circle corresponds to a single cell. Δ*yoaI* cells are depicted in red, while wild-type cells are in gray. The cultures were grown in supplemented minimal A medium containing either 10mM (no stress) or no added magnesium (Mg^{2+} stress). Data are derived from three independent replicates and the number of cells analyzed is indicated by (n). Mean fluorescence is shown with blue bars and is noted in blue text. P-values indicate the results of a t-test when Δ*yoaI* cells were compared to the wild-type cells, ****P ≤ 0.0001, ***P ≤ 0.001, and "ns" = P > 0.05. (C) Schematic representation of small membrane protein YoaI as a connector of the two-component systems, PhoR-PhoB and EnvZ-OmpR. YoaI is transcriptionally controlled by the PhoR-PhoB system, under low Mg^{2+} YoaI protein levels increase and it binds sensor kinase EnvZ and modulates signaling through the EnvZ-OmpR pathway. (Also see Fig. S9)

1237 **Table 1. Summary of the 17 small proteins induced under low magnesium stress in *E. coli*.** Small proteins with at least a 3-fold increase in
1238 reads mapping to the translation initiation site under low Mg^{2+} relative to no stress are indicated below. The analysis of transcriptional regulation,
1239 localization, and characterization of deletion and overexpression phenotypes is summarized.

Small protein	Transcriptional Regulation		Membrane localization	Phenotypic characterization	
				Deletion	Overexpression
MgtS	+	PhoQP-dependent, in an operon *mgtS-mgtT*	Y	No effect	Growth defect (prolonged lag phase) & decrease in cell size during lag and exponential phase
MgrB	+	PhoQP-dependent	Y	Increase in cell length, and change in colony morphology (larger, rough, translucent colonies) (Yadavalli *et al*, 2016)	Growth defect (prolonged lag phase) & increase in cell size during lag phase
PmrR	+	BasSR-dependent (Chen *et al*, 2021; Kato *et al*, 2012)	Y	Growth defect (lower yield at saturation)	Growth defect (prolonged lag phase) & decrease in cell size during lag phase
MgtT	+	PhoQP-dependent, in an operon *mgtS-mgtT*	N	No effect	No effect
YmiC	+	PhoQP-dependent, in an operon *ymiA-yciX-ymiC*	Y	No effect	No effect
YmiA	+		Y	No effect	Growth defect (prolonged lag phase) & increase in cell length during lag phase
YoaI	-	PhoRB-dependent (Fitzgerald *et al*, 2023; Yoshida *et al*, 2012; Chekabab *et al*, 2014)	Y	No effect	Growth defect (prolonged lag phase) & decrease in cell size during lag phase
YobF	-		Y	Growth defect (lower yield at saturation)	No effect
YddY	+	PhoQP-dependent	N	No effect	No effect
YriB	+	PhoQP-dependent, in an operon *yriA-yriB*	N	Growth defect (lower yield at saturation)	No effect
YadX	+	PhoQP-dependent, in an operon *yadX-clcA-yadW*	N	No effect	No effect
YkgS	-		N	No effect	Growth defect (slow growth) & increase in cell length during exponential phase
YriA	+	PhoQP-dependent, in an operon *yriA-yriB*	N	No effect	No effect
YdgU	+	PhoQP-dependent, in an operon *asr-ydgU*	Y	No effect	No effect
YqhI	+		N	No effect	No effect
YadW	+	PhoQP-dependent, in an operon *yadX-clcA-yadW*	N	No effect	No effect
DinQ	-		Y	No effect	Growth defect (slow growth)

1240 '+' indicates transcriptional upregulation and '-' indicates no change in transcriptional activity under magnesium stress vs. no stress; 'Y' indicates proteins predicted to
1241 contain membrane helices and shown to localize to the membrane, 'N' indicates a lack of membrane helices based on bioinformatic prediction (see Methods for details)